GEOLOGICA CARPATHICA, DECEMBER 2011, 62, 6, 547–562 doi: 10.2478/v10096-011-0039-2

Quaternary post-collision alkaline volcanism NW of Ahar (NW Iran): geochemical constraints of fractional crystallization process

RAHIM DABIRI[1*], MOHAMAD HASHEM EMAMI[2], HABIB MOLLAEI[3], BIN CHEN[4], MANSOR VOSOGI ABEDINI[1], NEMATALLAH RASHIDNEJAD OMRAN[5] and MITRA GHAFFARI[3]

[1]Department of Geology, Science and Research Branch, Islamic Azad University, Tehran, Iran; * r.dabiri@srbiau.ac.ir
[2]Department of Geology, Islamshahr Branch, Islamic Azad University, Islamshahr, Iran
[3]Department of Geology, Mashhad Branch, Islamic Azad University, Mashhad, Iran
[4]School of Earth and Space Sciences, Peking University, Beijing 100871, P. R. China
[5]Department of Geology, Tarbiat Modares University, P.O. Box 14115-175, Tehran, Iran

(Manuscript received January 5, 2011; accepted in revised form June 9, 2011)

Abstract: Major and trace elements and Sr–Nd isotopic data are presented for the Quaternary alkaline volcanism NW of Ahar (NW Iran). The exposed rocks mainly consist of alkali basalts, trachybasalts, basaltic trachyandesites and trachyandesites. Alkali basalts and trachybasalts display microlithic porphyritic texture with phenocrysts of olivine, clinopyroxene, and plagioclase in microlithic groundmass. In the more evolved rocks (basaltic trachyandesites and trachyandesites), amphibole and biotite have appeared. Major and trace element abundances vary along continuous trends of decreasing MgO, TiO_2, $Fe_2O_3^*$, CaO, Co, Cr, V and Zn, and increasing K_2O, Al_2O_3, Ba and Th with increasing SiO_2. The Sr and Nd isotopic ratios vary from 0.704463 to 0.704921 and from 0.512649 to 0.512774, respectively. Alkali basalts with high $^{143}Nd/^{144}Nd$ ratio, low $^{87}Sr/^{86}Sr$ ratio and high MgO, Ni and Cr contents indicate that they were generated from relatively primitive magmas. Ba, Cr and La/Sm ratios versus Rb suggest that fractional crystallization of alkali basalts could have played a significant role in the formation of evolved rocks. Assimilation and fractional crystallization modelling, as well as Rb/Zr, Th/Yb and Ta/Yb ratios clearly indicate that crustal contamination accompanied by the fractional crystallization played an important role in petrogenesis of the trachyandesites. The small compositional differences between magma types, isotopic composition, mineralogy and nonlinear trends on Harker diagrams also indicate that magma mixing was not an essential process in the evolution of the Ahar magmas. Petrogenetic modelling has been used to constrain sources. Trace element ratio plots and REE modelling indicate that the alkali basalts were generated from a spinel-peridotite source via small degrees (~2.5%) of fractional melting.

Key words: Quaternary, Iran, NW Ahar, geochemistry, alkaline volcanism, crustal contamination.

Introduction

The Quaternary alkaline volcanism of NW Iran has been closely linked to the collision between the Afro-Arabian and Eurasian plates. The northward motion of the Afro-Arabian plate in the Late Mesozoic and Early Cenozoic was associated with subduction under the southern margin of Eurasia (e.g. Şengör & Yilmaz 1981; Ricou 1994; Mohajjel et al. 2003; Agard et al. 2005; Azizi & Moinevaziri 2009; Saki 2010). Four structural zones developed in Iran as a result of Neo-Tethys subduction beneath the Central Iran Microplate (CIM) and the following collision of the Iranian and Afro-Arabian plates (Fig. 1a). These structural zones include the Urumieh-Dokhtar magmatic arc (UDMA), Sanandaj–Sirjan Metamorphic Zone (SSMZ) and folded Zagros Zone (High Zagros and Zagros Simply Folded Belt) (Alavi 2004). The UDMA represents a continental arc that formed as a result of the subduction of the Neotethyan oceanic crust under the SSMZ in the Late Mesozoic (Alavi 1994).

This magmatic belt contains volcanic and plutonic rocks of Eocene–Quaternary age that extend from NW to SE in Iran. Magmatic activity in the UDMA started in the Late Cretaceous and continued during the Eocene until Quaternary period (Ahmadzadeh et al. 2010). However, the peak of magmatic activity is thought to be of Eocene age (e.g. Stocklin 1974; Farhoudi 1978; Emami 1981; Jahangiri 2007). Geochemical studies indicate that the Urumieh-Dokhtar magmatic arc is generally composed of subduction-related calc-alkaline rocks (e.g. Jung et al. 1976; Dupuy & Dostal 1978; Berberian et al. 1982; Azizi & Jahangiri 2008). Alkaline rocks are also reported locally by Amidi et al. (1984), Hassanzadeh (1993), Moradian et al. (1997), Hajalilou et al. (2009), Khairkhah et al. (2009), Saadat et al. (2010), Saadat & Stern (2011). These researchers have discussed the geochemistry, origin, magmatic processes (such as fractional crystallization, crustal contamination and magma mixing), age and tectonic settings of Quaternary volcanic rocks in Iran. The younger volcanic activity in the Urumieh-Dokhtar magmatic arc is mainly alkaline in nature and is associated with tectono-magmatic processes related to post-collisional, intra-continental rifting events (Richards 2003). In this paper, we present new geochemical characteristics and Sr, Nd data on lavas from the Quaternary alkaline volcanism in northwest Iran, filling a gap in the knowledge of the post-

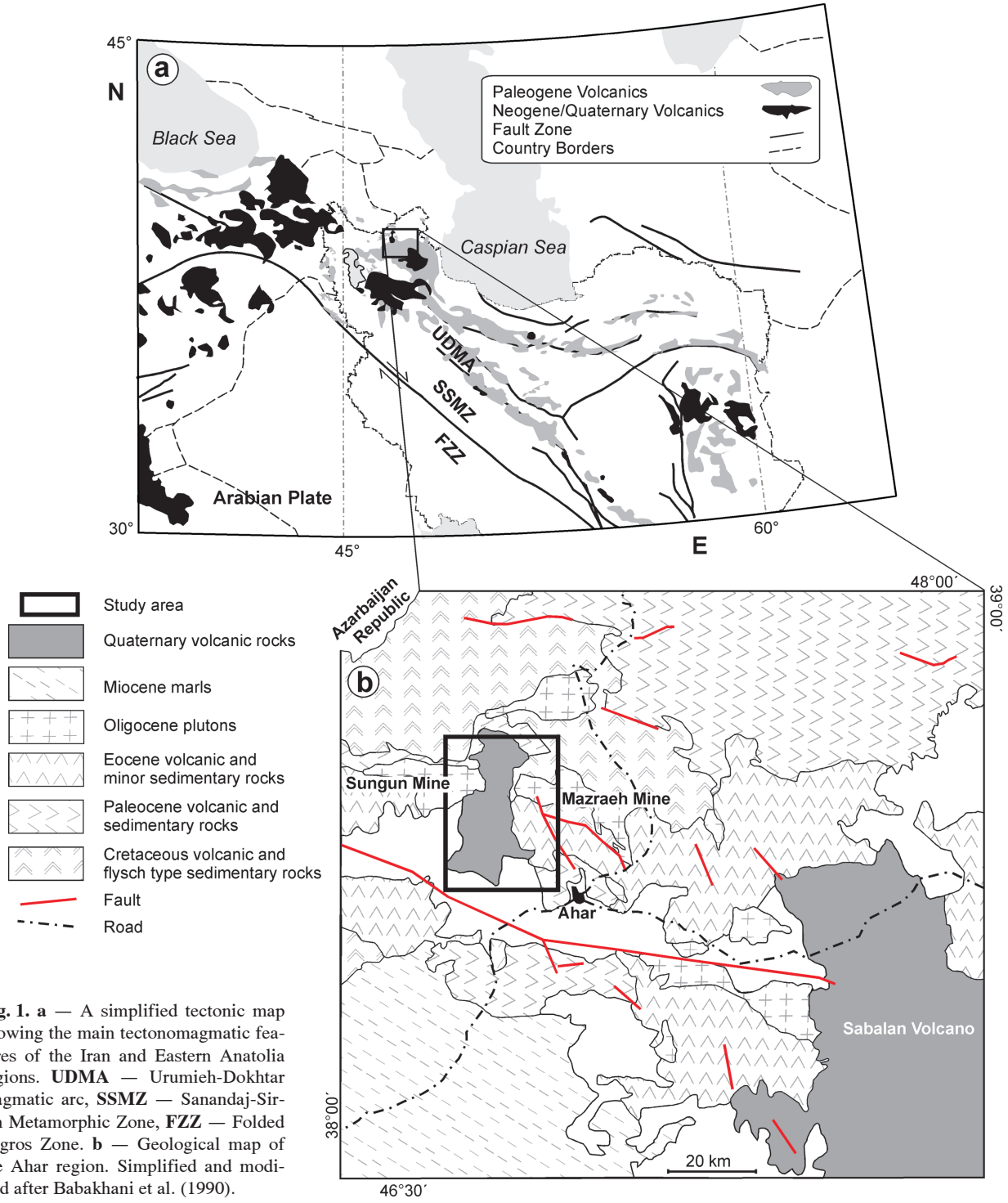

Fig. 1. a — A simplified tectonic map showing the main tectonomagmatic features of the Iran and Eastern Anatolia regions. **UDMA** — Urumieh-Dokhtar magmatic arc, **SSMZ** — Sanandaj-Sirjan Metamorphic Zone, **FZZ** — Folded Zagros Zone. **b** — Geological map of the Ahar region. Simplified and modified after Babakhani et al. (1990).

collisional magmatism in NW Iran. We use these data to infer the petrogenesis of these rocks in order to interpret their melt sources and magmatic evolution.

Geological setting

The study area is located in NW Ahar, NW Iran (Fig. 1b). In the classification of the structural units of Iran, this area is a part of the Central Iranian magmatic arc (UDMA) (Fig. 1a). A simplified geological map of NW Ahar is shown in Fig. 2. The composition of volcanic rocks in this area varies from calc-alkaline to alkaline during the Eocene to Quaternary. The Quaternary volcanism is represented by lava flows (Fig. 2). The volcanic sequences in the Ahar area are correlatable with the eastern part of Turkey. According to the study of Alberti et al. (1980), Innocenti et al. (1982), Moinevaziri (1985), Mitchell et al. (1999) and Jamali et al.

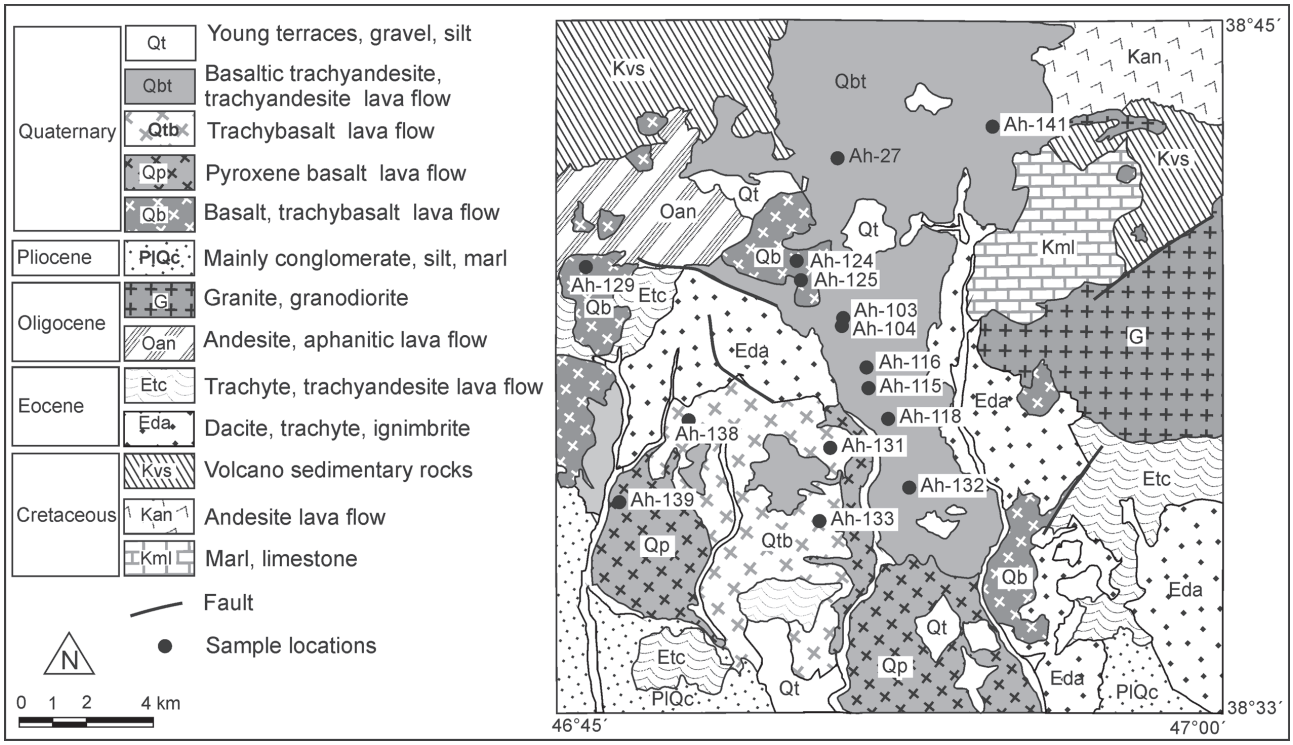

Fig. 2. A modified and simplified geological map (after Mehrpartou 1993) of the NW Ahar. The led circles show the sample locations.

(2010) the last phase of volcanic activity in this area occurred in Quaternary. The oldest unit of this region is Cretaceous (?) basement metamorphic rocks (micaschist, meta-diabase and amphibolite), that is exposed in a very limited area. These rocks are covered by the Upper Cretaceous volcanic and flysch type sedimentary rocks (Fig. 1b). The Cenozoic magmatism started in the Paleocene and continued in the Eocene with intensive volcanic activity that produced widespread intermediate to felsic rocks. In the Oligocene–Miocene large granitoid plutons were emplaced and this caused extensive alteration and mineralization (Mollaei 1993; Mollaei et al. 2009). The Oligocene-Miocene intrusions mostly consist of coarse- to medium-grained granodiorite and monzonite, with local, younger diorite and gabbro plutons. More alkaline, nepheline-syenitic to monzosyenitic bodies occur in Kaleybar and Razghah (in NW of Iran) (Ashrafi 2009; Aghazadeh 2009; Tajbakhsh 2010). The Quaternary basaltic and trachyandesitic rocks unconformably cover the older magmatic units. This Quaternary alkaline volcanism in northwest Iran occurred after Late Miocene calc-alkaline magmatism (Jahangiri 2007). During the Late Miocene to Quaternary, the Ahar-Arasbaran region, underwent regional contraction, shortening first in the N-NW direction and subsequently in the NNE direction. The NNE-oriented crustal shortening was accompanied by WNW stretching and extension and associated intensive alkaline magmatism in a broad zone of dextral transtension in the hinterland of the Arabia–Eurasia collision front (Mohajjel & Fergusson 2000; Sosson et al. 2005; Masson et al. 2006; Dilek et al. 2010; Jamali et al. 2010).

Analytical techniques

A total of about 200 samples from Quaternary alkaline rocks in the NW of Ahar were collected. One hundred twenty thin sections were studied by Polarized microscope. Fifteen representative samples were then selected for whole-rock chemical analysis (Table 1). Samples weighed between 1–1.5 kg before crushing and powdering. Whole-rock major elements were determined by X-ray fluorescence spectrometer (XRF) and trace and rare earth elements (REE) were determined by lithium borate fusion ICP-MS at the ALS Chemex Laboratories in Vancouver, Canada.

Sr and Nd isotopic analyses were performed at the Institute of Geology and Geophysics (IGG) in Beijing, China. Mass analyses were performed with a multi-collector VG354 mass spectrometer. Rb, Sr, Sm and Nd concentrations were measured using the isotopic dilution method. $^{87}Sr/^{86}Sr$ and $^{143}Nd/^{144}Nd$ ratios were normalized against $^{86}Sr/^{88}Sr = 0.1194$ and $^{146}Nd/^{144}Nd = 0.7219$, respectively. $^{87}Sr/^{86}Sr$ ratios were adjusted to NBS-987 Sr standard = 0.710250 and $^{143}Nd/^{144}Nd$ ratios to La Jolla Nd standard = 0.511860. Uncertainties resulting from the concentration prior to isotopic dilution are ±2 % for Rb, ±0.4–1 % for Sr and less than ±0.5 % for Sm and Nd, depending upon the concentration levels.

Petrographic studies

The volcanic rocks in the study area, according to mineral assemblages, can be divided into three sub-groups, based on the

Table 1: Representative whole-rock analyses of the Ahar Quaternary volcanic rocks. **AB** — alkali basalt, **TB** — trachybasalt, **BTA** — basaltic trachyandesite, **TA** — trachyandesite.

Sample	Ah-124	Ah-125	Ah-138	Ah-139	Ah-129	Ah-131	Ah-133	Ah-115	Ah-116	Ah-132	Ah-141	Ah-103	Ah-104	Ah-118	Ah-27
Rock type	AB	AB	AB	AB	TB	TB	TB	BTA	BTA	BTA	BTA	TA	TA	TA	TA
SiO_2 (wt. %)	48.40	45.60	47.71	46.60	48.68	49.50	50.50	52.32	53.10	51.04	51.90	56.13	53.90	56.69	54.70
TiO_2	1.96	3.16	2.94	2.31	1.62	1.74	1.52	1.07	1.02	1.21	0.95	1.02	0.67	0.71	0.49
Al_2O_3	15.09	15.50	14.97	15.73	15.96	15.50	17.40	18.05	18.50	15.00	16.45	18.90	18.63	18.55	19.40
Fe_2O_3	8.93	9.34	9.05	9.65	9.40	8.40	8.60	6.89	7.25	8.22	7.98	4.56	5.70	5.06	5.61
MnO	0.15	0.14	0.12	0.22	0.14	0.13	0.12	0.15	0.14	0.11	0.15	0.14	0.11	0.07	0.07
MgO	7.31	8.08	8.30	8.40	6.07	5.69	4.60	3.32	2.28	3.89	4.50	1.75	2.78	1.14	1.82
CaO	9.44	9.96	8.30	9.13	9.22	8.63	8.78	8.37	6.20	7.80	7.47	5.32	6.43	4.20	5.40
Na_2O	3.66	2.40	2.56	2.61	4.20	4.22	4.10	4.60	5.02	4.33	3.64	6.36	6.20	5.09	6.09
K_2O	0.97	1.56	1.48	1.58	1.95	1.60	1.36	2.76	3.10	2.87	2.25	3.04	3.36	2.73	2.77
P_2O_5	0.33	0.46	0.39	0.32	1.00	0.86	0.93	0.62	0.64	1.16	0.59	0.47	0.37	0.27	0.23
LOI	0.49	1.50	2.20	1.27	1.08	2.10	0.89	1.05	1.06	2.27	3.08	1.49	1.27	1.59	1.09
Total	96.73	97.70	98.01	97.82	99.32	98.37	98.80	99.20	98.31	97.90	98.96	99.18	99.42	96.10	97.67
Cs (ppm)	1.09	0.60	0.32	0.11	1.23	0.49	0.43	1.46	2.16	0.33	0.38	2.31	1.84	3.00	2.01
Rb	35.2	33.3	37.5	34.6	40.6	39.5	40.0	43.0	45.6	44.8	44.0	54.6	51.7	57.6	49.7
Ba	335	363	520	371	707	473	568	874	1020	944	708	1058	1190	1118	1082
Th	1.48	2.29	1.91	1.86	2.57	2.57	3.47	4.27	3.89	3.09	5.13	5.13	7.08	5.25	7.24
Ta	1.0	1.1	1.2	0.9	1.6	1.3	1.2	1.3	1.3	1.1	1.3	1.1	1.7	0.7	0.8
Nb	19.3	21.0	25.6	17.1	32.5	27.6	26.1	23.8	24.1	24.7	23.1	17.7	24.9	11.8	12.5
Sr	715	830	550	422	1430	1695	1445	1190	1300	1850	1450	2324	1604	1952	2180
Pb	5	9	11	10	11	8	8	17	18	8	11	13	18	15	18
Zr	268	260	249	253	207	253	204	189	136	168	158	160	154	96	85
Hf	4.2	4.1	3.7	2.5	4.5	3.8	3.5	4.5	4.5	4.0	5.7	4.2	5.4	3.2	3.3
Y	19.3	17.4	14.2	21.6	18.8	15.8	15.6	20.2	20.8	11.7	28.0	15.5	14.2	13.0	10.1
V	185	186	218	268	190	212	199	182	171	203	176	176	97	107	71
Cr	320	330	347	296	291	254	209	153	109	161	155	80	74	66	90
Co	35.4	42.1	28.7	30.7	39.5	45.9	25.7	23.7	21.1	29.1	22.4	14.3	20.4	14.3	15.3
Ni	266	244	286	215	185	174	181	159	186	177	162	36	59	16	28
Zn	106	130	121	95	124	130	118	99	79	142	95	51	85	54	63
La	44.8	50.1	43.0	50.0	63.5	56.3	42.4	42.4	50.1	44.2	75.0	46.0	52.7	30.5	36.0
Ce	37.8	58.0	53.7	29.5	97.5	111.5	103.5	93.8	108.5	115.0	128.0	93.2	129.8	104.8	81.3
Pr	5.34	7.11	5.69	3.97	14.50	12.95	11.70	10.30	11.90	12.80	14.50	9.27	9.97	7.43	6.46
Nd	22.7	33.2	26.2	18.1	57.1	50.0	44.9	39.9	44.9	48.3	56.2	33.0	36.7	23.1	22.8
Sm	10.57	11.39	8.63	9.40	13.72	11.92	8.40	8.71	9.46	8.66	13.11	9.16	9.94	5.69	6.12
Eu	1.82	1.91	2.26	1.55	2.37	2.21	2.02	1.97	2.12	1.82	2.75	1.70	1.63	1.15	0.98
Gd	5.93	6.46	7.03	4.46	7.86	7.08	6.38	6.45	6.90	5.89	9.13	6.02	5.85	3.95	3.31
Tb	0.76	0.76	0.81	0.69	0.89	0.82	0.74	0.81	0.85	0.61	1.19	0.79	0.78	0.52	0.39
Dy	3.56	3.65	3.48	4.17	4.11	3.62	3.48	3.94	4.16	2.66	5.71	4.18	3.28	2.66	2.05
Ho	0.66	0.65	0.60	0.83	0.71	0.62	0.61	0.74	0.81	0.44	1.04	0.82	0.79	0.50	0.39
Er	1.80	1.86	1.65	2.41	1.96	1.64	1.71	2.16	2.27	1.23	2.96	2.46	2.34	1.46	1.12
Tm	0.23	0.23	0.18	0.32	0.24	0.18	0.19	0.27	0.30	0.14	0.37	0.31	0.33	0.19	0.13
Yb	2.73	2.91	2.50	2.50	3.40	2.89	2.00	1.91	2.15	2.00	3.00	1.90	2.10	1.20	1.40
Lu	0.34	0.28	0.27	0.37	0.22	0.17	0.18	0.29	0.31	0.14	0.37	0.26	0.17	0.20	0.16
$^{87}Sr/^{86}Sr$	0.704463	0.704697				0.704670			0.704800				0.704921		0.704763
$^{143}Nd/^{144}Nd$	0.512774	0.512742				0.512696			0.512702				0.512651		0.512649
ε_{Nd}	2.7	2.0				1.1			1.2				0.3		0.2

study of 120 samples. (I) Olivine basalt with grey to greyish brown colours, which displays vitrophyric, porphyritic and intersertal textures. Plagioclase, olivine and clinopyroxene form the main phenocryst phases in these basaltic rocks. The microcrystalline matrix is dominated by plagioclase, clinopyroxene and olivine. Rare nepheline also occurs in the groundmass of some olivine basalts; (II) Olivine trachybasalt to trachybasalt with porphyritic and trachytic textures occur. These samples contain plagioclase, clinopyroxene, biotite and olivine. Their groundmass consists of plagioclase, pyroxene, apatite and opaque minerals; (III) Amphibole trachyandesites are dark grey to black and have a trachytic, porphyritic and microlithic textures. Plagioclase, clinopyroxene, amphibole and biotite are ubiquitous phenocrysts. The groundmass consists of microlithes of plagioclase, amphibole and biotite with minor clinopyroxene.

Olivine occurs as phenocrysts and microphenocrysts in the basalt and trachybasalt. Some olivine phenocrysts are embayed and olivine also occurs as resorbed phenocrysts in the olivine basalts (Fig. 3a). There are reaction rims around olivine phenocrysts. The reaction rims around the olivines are composed of fine-grained orthopyroxene, plagioclase and Fe-Ti oxide.

Clinopyroxenes are found in all rock types as phenocrysts and microphenocrysts. In some clinopyroxene phenocrysts, matrix fills embayments and the others have embayed margins suggesting resorption (Fig. 3b). Clinopyroxene also occurs in glomeroporphyritic aggregates with plagioclase and Fe-Ti oxides.

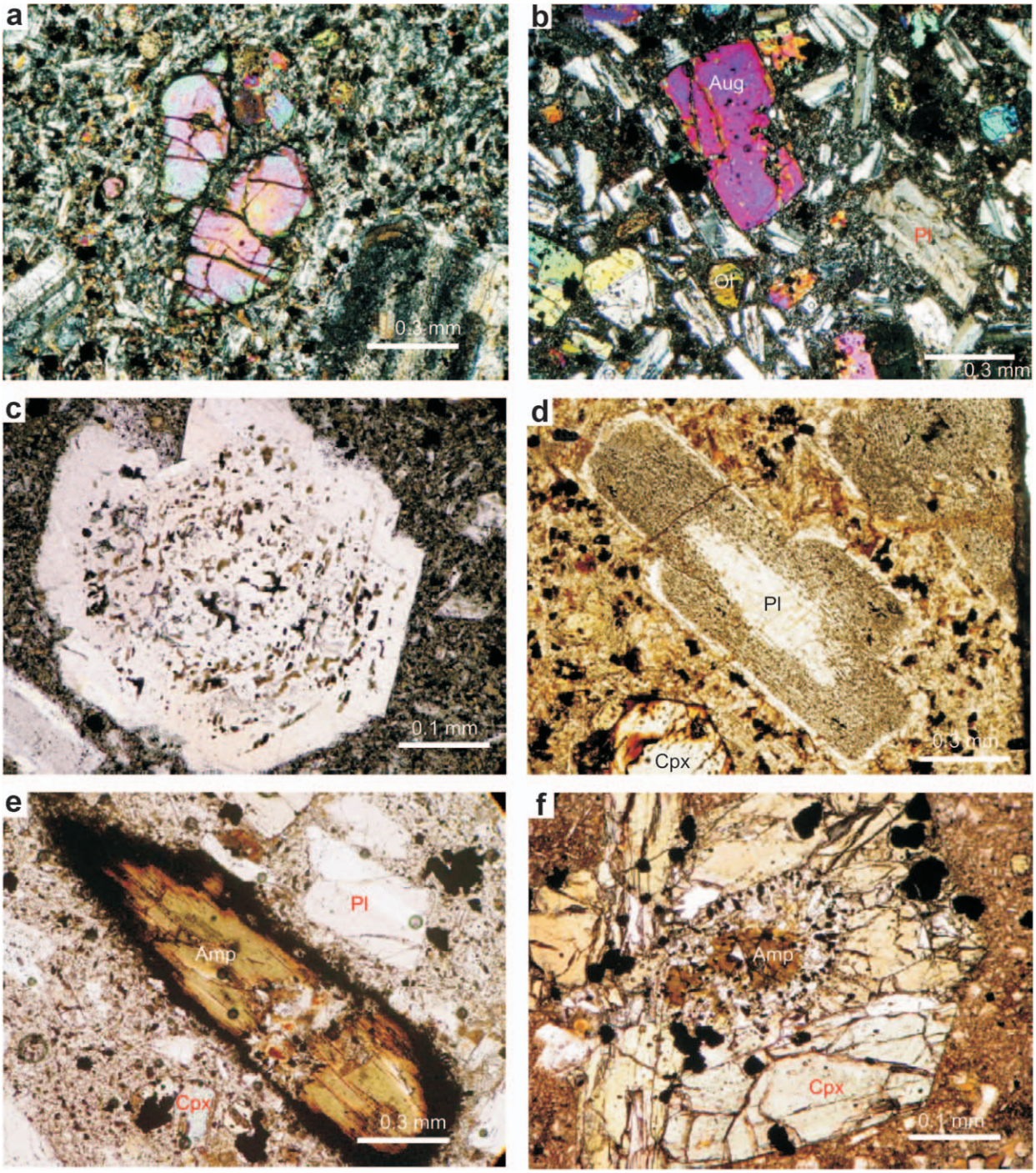

Fig. 3. a — Embayed olivine crystal in olivine basalt. **b** — Embayed augite crystal with melt inclusions; Aug — augite, Ol — olivine, Pl — plagioclase in olivine basalt. **c** — Sieve texture in a plagioclase phenocryst that has overgrown with clear rim in amphibole trachyandesite. **d** — Sieve texture in plagioclase phenocrysts with clear rim and core; Pl — plagioclase, Cpx — clinopyroxene in amphibole trachyandesite. **e** — Amphibole with thin rims of fine-grained Fe-Ti oxide, pyroxene and plagioclase; Amp — amphibole, Cpx — clinopyroxene, Pl — plagioclase in amphibole trachyandesite. **f** — Breakdown reaction of amphibole to clinopyroxene, plagioclase and Fe-Ti oxides. Big crystals of Cpx around represent an overgrowth; Cpx — clinopyroxene, Amp — amphibole in amphibole trachyandesite.

Plagioclase phenocrysts show clear evidence of multiple evolution and periods of dissolution and growth. On the basis of textural criteria, plagioclase phenocrysts can be identified as one of three types: (a) unsieved, with no dissolution texture, (b) sieve-cored, where the cores are riddled with glass and overgrown with clear rims (Fig. 3c), and (c) sieve-ringed, where a clear core is mantled by a resorption zone followed by a clear rim (Fig. 3d).

Amphibole occurs as yellowish green to yellowish brown pleochroism phenocrysts, that are observed as reacted pheno-

crysts. They typically have thin rims of fine-grained pyroxene and Fe-Ti oxide (Fig. 3e). This feature probably reflects volatile loss during ascent of magma in conduits (Rutherford & Hill 1993). Occasionally, amphiboles breakdown to clinopyroxene, plagioclase and Fe-Ti oxides in trachyandesite (Fig. 3f). In some amphibole phenocrysts, groundmass microlithes fill embayments. The biotites, typically euhedral grains, occur as elongated crystals surrounded by opaque grains at the rim. Fe-Ti oxides have magnetite compositions, are subhedral and are present mainly in association with mafic minerals and disseminated in the groundmass.

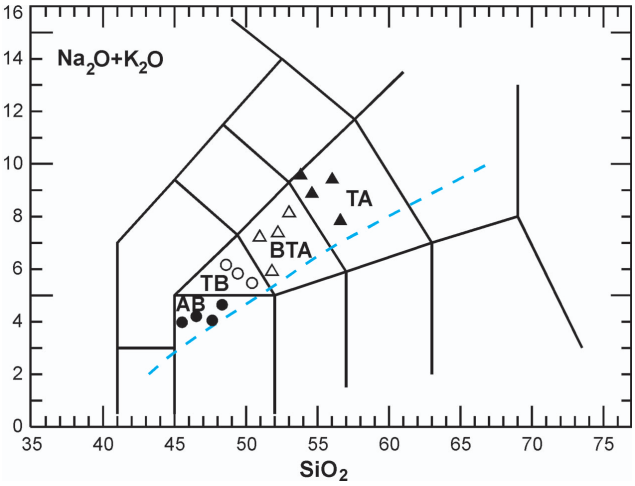

Fig. 4. Total alkali-silica diagram (Le Maitre et al. 1989) for the NW Ahar Quaternary volcanic rocks. Dividing line between alkaline and subalkaline fields after Irvine & Barager (1971). **AB** — alkali basalt, **TB** — trachybasalt, **BTA** — basaltic trachyandesite, **TA** — trachyandesite.

Geochemistry

Major and trace elements

Major and trace elements analyses were carried out on fifteen samples (Table 1). The Quaternary volcanic rocks in Ahar have a wide range of chemical composition with SiO_2 contents ranging between 45 % and 57 %, and have been classified on the basis of their alkali and silica contents using the total alkali–SiO_2 diagram (TAS) of Le Maitre et al. (1989). No major compositional gap or bimodality is observed; instead, all the samples lie along a well defined and relatively tight trend in the TAS diagram (Fig. 4). On this diagram the composition of volcanic rocks is represented by alkali basalt, trachybasalt, basaltic trachyandesite and trachyandesite. This diagram also shows that all samples are plotting in the alkaline field. In the Harker diagrams, as SiO_2 increases, Fe_2O_3, MgO, CaO and TiO_2 decrease, while K_2O and Al_2O_3 increase (Fig. 5). Such negative and positive correlations can be explained by removal of the ferromagnesian phases such as olivine and pyroxene. Compatible trace elements such as Cr, Co, V and Zn show strong negative correlation with increasing SiO_2, whereas incompatible trace elements (e.g. Ba, Th) correlate positively (Fig. 6). These major and trace element trends are broadly consistent with fractional crystallization plagioclase + pyroxene + Fe-Ti oxides + amphibole + biotite removal, all of which are present as phenocrysts in the Quaternary volcanic rocks in Ahar. Primitive mantle-normalized trace elements patterns of the study area are characterized by a Nb–Ta trough and are enriched in incompatible trace elements (Fig. 7). The negative Nb–Ta anomaly for Ahar lavas is consistent with a melt source that was metasomatized by Nb–Ta-depleted aqueous fluids produced from a dehydrating slab with residual rutile.

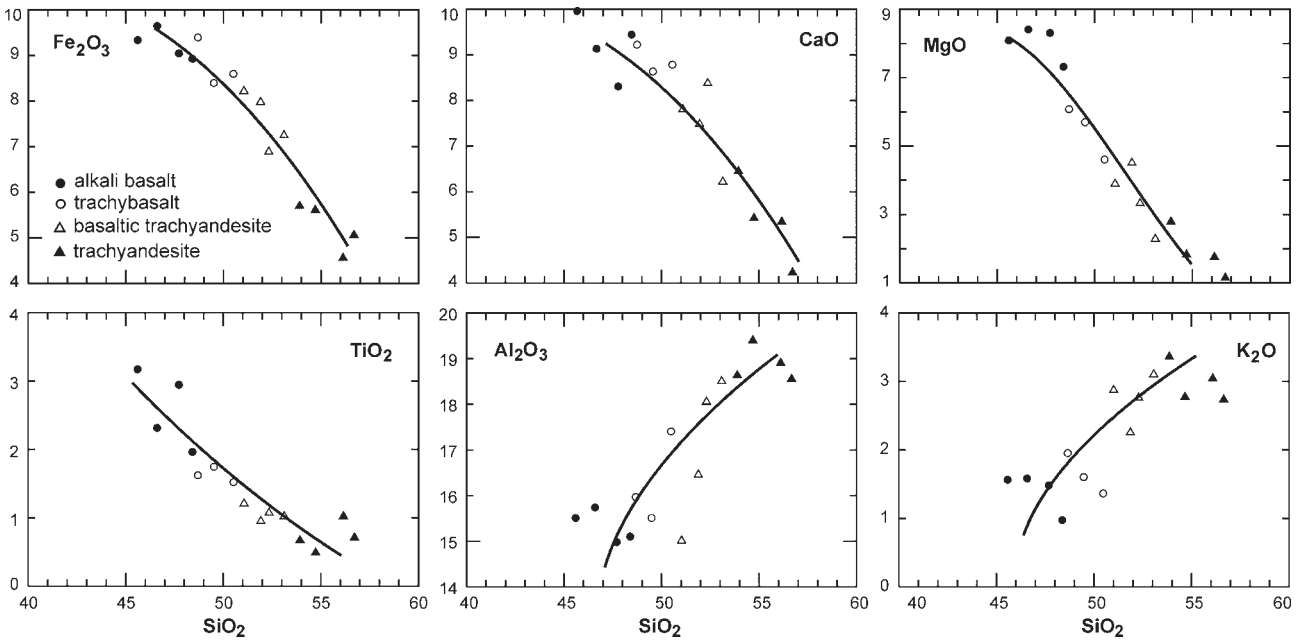

Fig. 5. Selected major element variations against SiO_2 content.

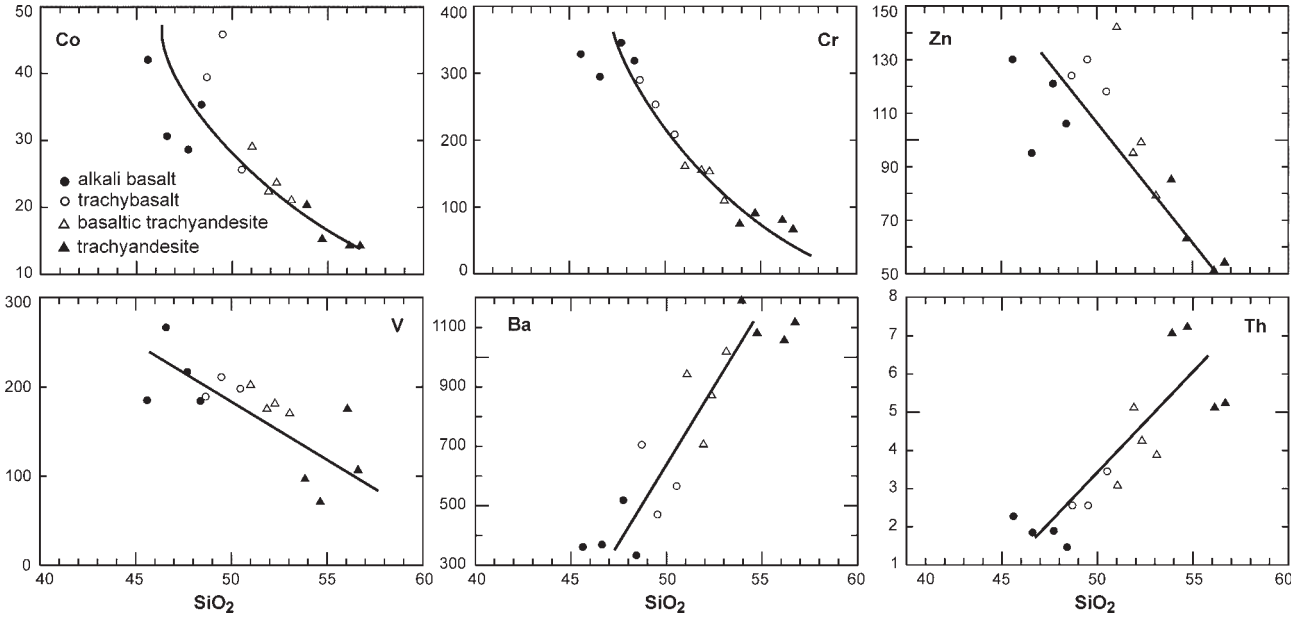

Fig. 6. Selected trace element variations against SiO_2 content.

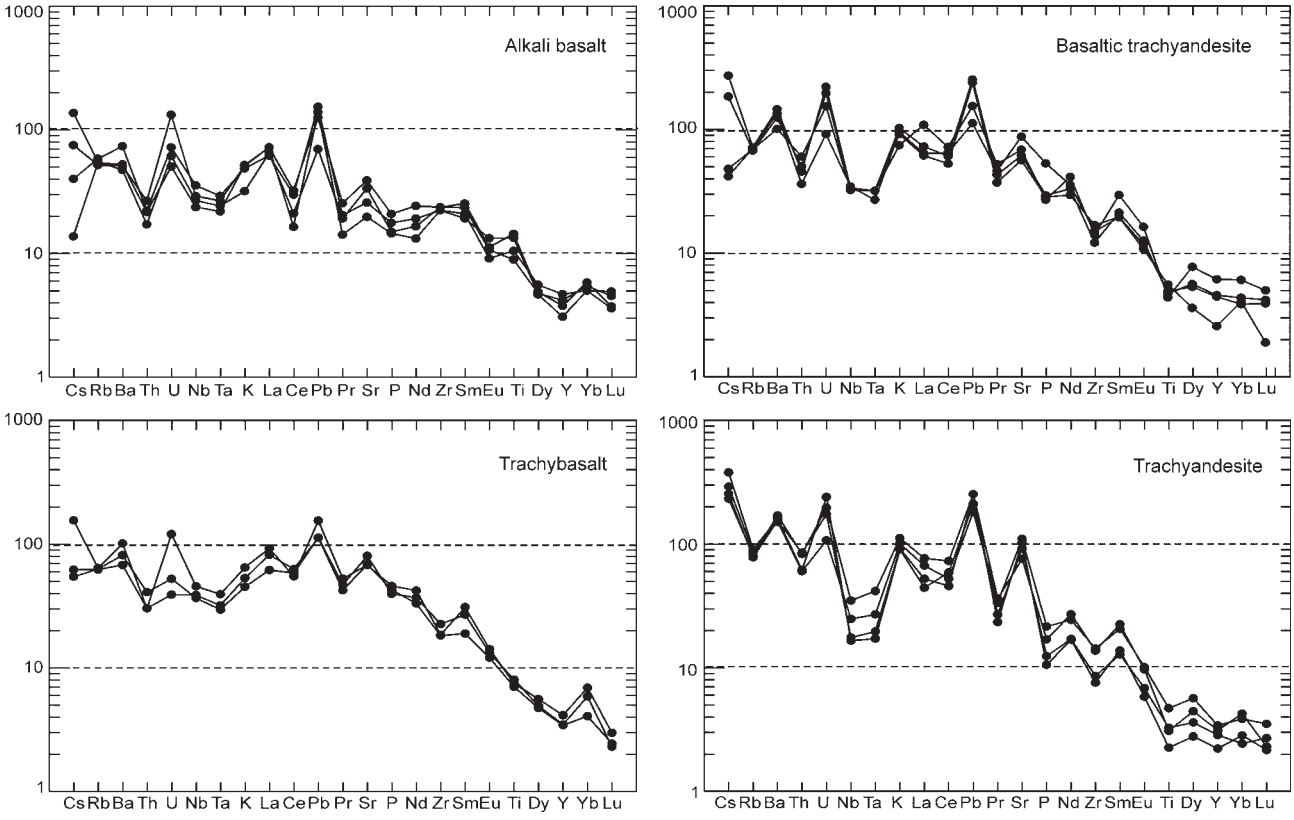

Fig. 7. Primitive mantle normalized alkali basalt, trachybasalt, basaltic trachyandesite and trachyandesite patterns for the Ahar Quaternary volcanic rocks (normalized values from Sun & McDonough 1989).

When compared with the multi-element diagrams of the study area volcanic rocks, alkali basalts are characterized by a less marked enrichment in Rb, Ba, Th, K, Sr (Fig. 7). Enrichment in Rb, Ba, Th, K, Sr, Zr, Hf, Pb, Ta, LREE (La, Ce) and negative anomalies in Co, V, Zn, Ti, Ni, Cu in the more differentiated rocks (trachybasalts, basaltic trachyandesites and trachyandesites) suggests that these rocks derived from the alkali basalts.

Isotope geochemistry

Six samples have been analysed for Sr and Nd isotopes. Sr and Nd isotope ratios determined in this study are presented in Figure 8, and representative analyses and ε_{Nd} values are listed in Table 1. The Nd isotopic compositions of $^{87}Sr/^{86}Sr$ ratios range from 0.704463 to 0.704921; $^{143}Nd/^{144}Nd$ ratios range from 0.512649 to 0.512774. The ε_{Nd} values range Nd from 0.2 to 2.7. There is a clear relationship between geochemistry type and isotopic characteristics. In the conventional $^{143}Nd/^{144}Nd$ vs. $^{87}Sr/^{86}Sr$ diagram (Fig. 8), the alkali basalts plot in the depleted quadrant of the mantle array, whereas the trachyandesites plot in the enriched side. Basaltic trachyandesites and trachybasalts lie between the alkali basalts and trachyandesites (Fig. 8). All the samples plot within the mantle array and close to the field of BSE (Bulk Silicate Earth). This suggestion is compatible with the ε_{Nd} values of the rocks, because a positive value of epsilon for volcanic rocks implies a magma derived from an isotopically depleted source (e.g. Rollinson 1993). Low $^{87}Sr/^{86}Sr$ and high $^{143}Nd/^{144}Nd$ and low Ba and Rb in contents indicate a mantle source also for these rocks. The higher $^{87}Sr/^{86}Sr$ and the lower $^{143}Nd/^{144}Nd$ isotope ratios of the trachyandesites may be interpreted in terms of crust–magma interaction. Sr–Nd isotopic compositions were compared with data of young volcanics from north Iran and east Turkey (Fig. 8). The isotopic data of the Ahar Quaternary volcanic rocks are similar to the isotopic data reported from the Damavand Quaternary stratovolcano (Liotard et al. 2008; Mirnejad et al. 2010) in the central part of the Alborz magmatic belt (AMB), Quaternary volcanism from the Iran/Turkey borderlands (Kheirkhah et al. 2009) and Quaternary volcanic centers in Eastern Anatolia (Buket & Temel 1998). The isotopic ratio of the Lesser Caucasus alkaline Quaternary volcanic rocks (Lebedev et al. 2003, 2007), Ararat Quaternary volcano (Gülen 1984) and Neogene volcanic rocks of eastern Turkey (Aydin et al. 2008) are different from the study rocks (Fig. 8). The Ahar Quaternary volcanic rocks have high $^{87}Sr/^{86}Sr$ and low $^{143}Nd/^{144}Nd$ compared to the Caucasus alkaline Quaternary volcanic rocks and Ararat Quaternary volcano and low $^{87}Sr/^{86}Sr$ compared to the Neogene volcanic rocks of eastern Turkey.

Discussion

Fractional crystallization

The new data reported in this study indicate that the Quaternary volcanic rocks in Ahar have similar petrographical and geochemical features and define typical alkaline trends from alkaline basalts to trachyandesites. Major element variations are mainly controlled by the fractionation of olivine and clinopyroxene, which strongly deplete the magma in MgO, TiO_2, $Fe_2O_3^*$, CaO and compatible trace elements (e.g. Co, Cr, V and Zn) (Figs. 5, 6). Incompatible (Rb) versus incompatible (Ba) trace element variations are linear,

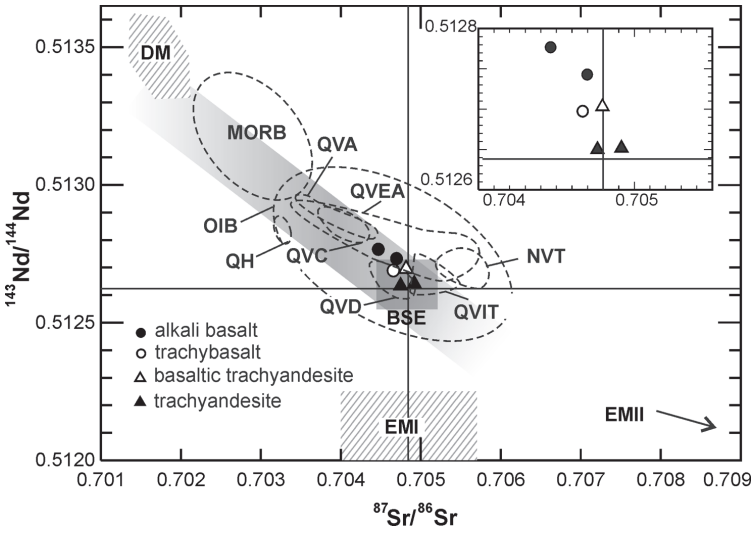

Fig. 8. $^{143}Nd/^{144}Nd$ and $^{87}Sr/^{86}Sr$ isotope variation diagram for the Ahar Quaternary volcanic rocks. BSE (Bulk Silicate Earth) composition is from Hart et al. (1992). Locations of depleted mantle (DM) and enriched mantles (EMI, EMII) are from Zindler & Hart (1986). The samples from other Neogene alkaline volcanic suites are also plotted for comparison, including the QVA (alkaline Quaternary volcanic rocks, Ararat volcano; Gülen 1984), QVC (alkaline Quaternary volcanic rocks, Lesser Caucasus; Lebedev et al. 2003, 2007), QVD (alkaline Quaternary volcanic rocks, Damavand Volcano; Liotard et al. 2008; Mirnejad et al. 2010), QVEA (Quaternary volcanic rocks, Eastern Anatolia; Buket & Temel 1998), QVIT (alkaline Quaternary volcanic rocks, Iran/Turkey borderlands; Kheirkhah et al. 2009), NVT (alkaline Neogene volcanic rocks, NE Turkey; Aydin et al. 2008) and QH (Hocheifel volcanic rocks, Germany; Fekiacova et al. 2007).

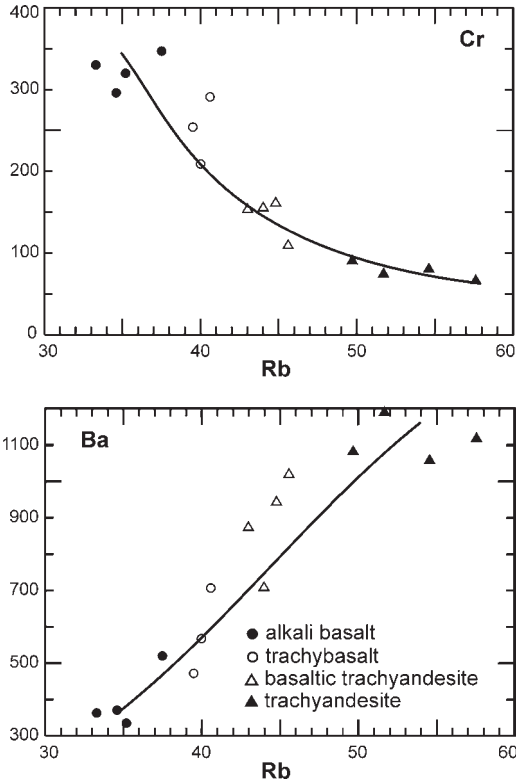

Fig. 9. Cr (compatible element) and Ba (incompatible element) against Rb for the Ahar Quaternary volcanic rocks.

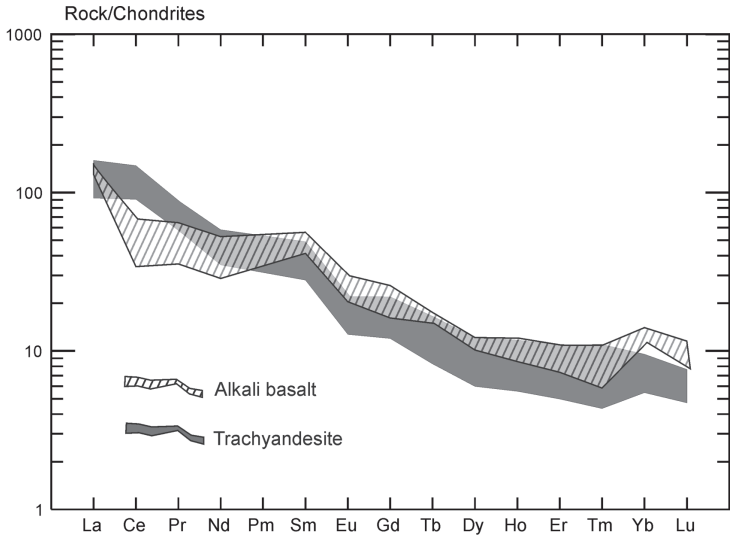

Fig. 10. Chondrite-normalized REE diagram for the alkali basalts and trachyandesites (normalized values after Nakamura et al. 1974).

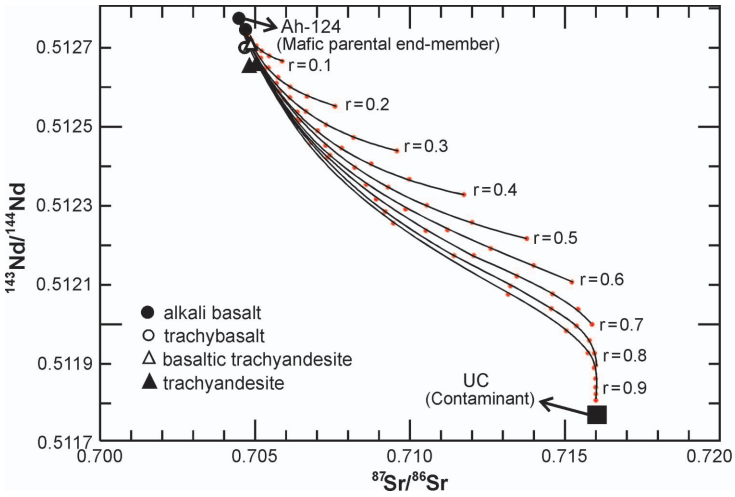

Fig. 12. AFC modelling for $^{87}Sr/^{86}Sr$ versus $^{143}Nd/^{144}Nd$ isotopic compositions for upper crustal (UC) end-member. Upper crustal values are from Veizer & Compston (1974) and O'Nions & Hamilton (1984). Variations in r (the ratio of the rate of assimilation/rate of crystallization) are shown with tick marks.

Table 2: Data used in the calculations of AFC modelling.

Starting composition*		Calculated bulk partition coefficient (D_o) **	K_d values for:				
			Olivine	Opx	Cpx	Plag	Mt
Sr	715	0.98	0.014	0.04	0.06	1.83	0.00
Nd	22.7	0.15	0.006	0.03	0.31	0.081	1.00
Th	1.48	0.015	0.04	0.13	0.03	0.01	0.00
Ta	1.0	0.07	0.04	0.15	0.013	0.018	1.00
Yb	2.73	0.2	0.014	0.34	0.62	0.067	0.9

K_d values are from Rollinson (1993) and Keskin (1994).

Abbrevations: **K_d** — mineral/melt partition coefficient, **Cpx** — clinopyroxene, **Plag** — plagioclase, **Mt** — magnetite. * — mafic parental end-member, sample Ah-124. ** — Of sample Ah-124 (Ol — 8 %, Opx — 1 %, Cpx — 18 %, Plag — 53 %, K-spar — 6 %, Mt — 5 %).

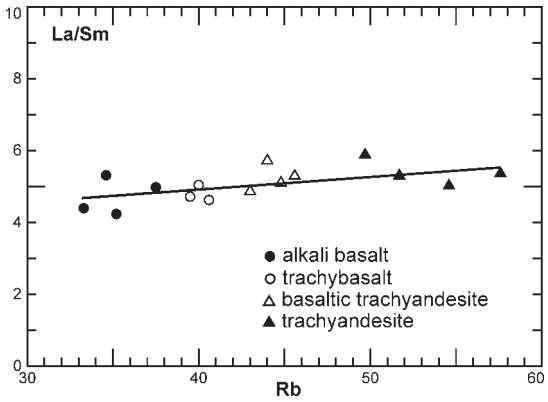

Fig. 11. La/Sm variations against Rb for the Ahar Quaternary volcanic rocks.

with trends from low abundances in alkali basalts towards higher abundances in trachyandesites (Fig. 9). Compatible (Cr) versus incompatible (Rb) element variations form curved rather than linear trends (Fig. 9). Normalized REE patterns form parallel trends, and LREE contents increase from alkali basalts to trachyandesites (Fig. 10). La/Sm data points (Fig. 11) plot along a line, a feature restricted to the process of fractional crystallization (Allegre & Minster 1978). The above-mentioned characteristics show that the Quaternary volcanic rocks in Ahar evolved predominantly through fractional crystallization of the petrographically observed phenocryst assemblage (olivine + plagioclase + clinopyroxene + amphibole + biotite + Fe-Ti oxides) and fractional crystallization is the dominant process for the Ahar rocks suite.

Role of crustal contamination

In order to constrain the role of crustal contamination, we have utilized the assimilation and fractional crystallization (AFC) model of DePaolo (1981). The negative trend in the Sr-Nd isotope diagram (Fig. 12) indicates that the magmas have been affected by crustal contamination during their ascent to the surface. We therefore attempted quantitative modelling of AFC using the equations of DePaolo (1981). In AFC modelling, the primitive mafic end-member is the alkali basalt sample Ah-124, which has a modal mineralogy of 8 % olivine, 1 % orthopyroxene, 18 % clinopyroxene, 53 % plagioclase, 6 % alkali feldspar, and 5 % magnetite from CIPW calculations (Table 2). It is further calculated from the CIPW values of the parent mafic end-member (Ah-124) that the bulk distribution coefficient for Sr is 1.12, and for Nd 0.10 (D_{Sr}=1.12; D_{Nd}=0.10). The upper crust has been selected for the contaminant end-member for the AFC modelling. Upper crustal values are from Veizer & Compston (1974) and O'Nions & Hamilton (1984). The ratios of the rate of assimilation to the rate of crystallization

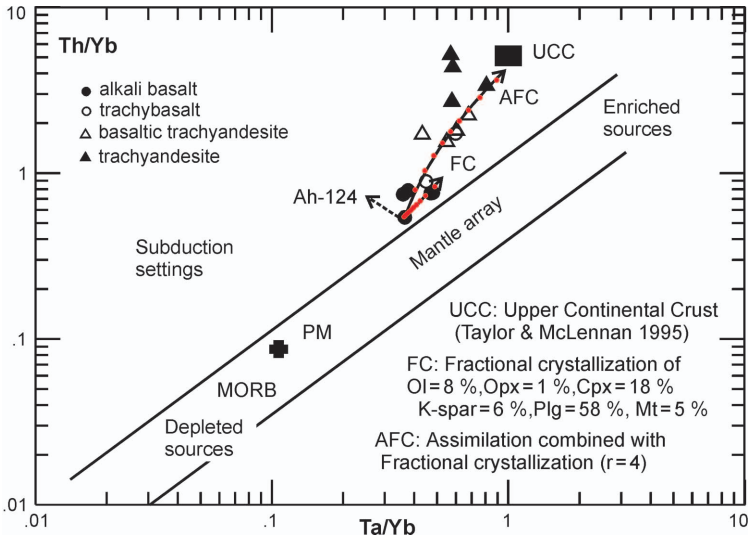

Fig. 13. Th/Yb vs. Ta/Yb diagram (after Pearce 1983) for the Ahar Quaternary volcanic rocks. **AFC** — assimilation and fractional crystallization, **C** — crustal contamination, **PM** — primordial mantle composition, **MORB** — Mid-Ocean Ridge Basalt.

(r values in Fig. 12) are from 0.1 to 0.9. Some samples are located along AFC trajectories. Alkali basalts exhibit negligible crustal contamination according to the diagram, since they are located along the r=0.1 trajectory (Fig. 12). The contamination of the primitive end-member Ah-124 by the continental crust gives rise first to trachybasalts and basaltic trachyandesites and then, by a higher degree of contamination, to trachyandesites.

We have also prepared AFC modelling for Th/Yb versus Ta/Yb diagram. This diagram has been found to be useful in the determination of crustal contamination (Fig. 13). Th is more affected than Ta and Yb during crustal contamination processes. Therefore, rocks with crustal contamination show high Th/Yb values (Wilson 1989). In this diagram, Yb is used as a normalizing factor to minimize the effects of fractional crystallization and crystal accumulation (Pearce 1983). The composition of the upper crust has also been plotted on the diagram. The fractional crystallization vector and AFC curve (r=0.4) for fractionation of a crystal assemblage consisting of 8 % olivine, 1 % orthopyroxene, 18 % clinopyroxene, 53 % plagioclase, 6 % alkali feldspar, and 5 % magnetite from the Ah-124 sample are also plotted (Fig. 13). The partition coefficients used are given in Table 2. The alkali basalt to trachyandesite lavas of the Ahar exhibit a consistent displacement from the mantle array towards higher Th/Yb values. The alkali basalts plot close to the mantle array field, suggesting minimal crustal contamination (Fig. 14). The trachyandesites have high ratios of Th/Yb (2.7–5.2). This suggests that the role of crustal contamination in their magma genesis cannot be ruled out.

The LILE (e.g. Rb and K) and Zr are incompatible with respect to the major crystallizing phenocryst assemblage (plagioclase, pyroxene, Fe-Ti oxides) and ratio like Rb/Zr do not significantly change by simple fractional crystallization of this assemblage. Variations in these ratios are preferably related to crustal contamination by AFC processes (Davidson et al. 1987). Examination of the study volcanic rocks shows that, in the alkali basalts, trachybasalts and basaltic trachyandesites, there is no significant variation in the Rb/Zr ratio (Fig. 14). The trachyandesites have a wider range of Rb/Zr values, which indicate that significant contamination is involved in the evolution of these samples. However, the trachyandesites have higher Sr and lower Nd isotope ratios, and have higher Th/Yb ratios and wider ranges in Rb/Zr values that clearly indicate crustal contamination, which has played an important role in the genesis of these rocks.

Magma mixing

Petrographic data provide evidence for magma mixing in the Quaternary volcanic rocks in Ahar. Some rocks contain disequilibrium mineral textures such as sieve textured plagioclases, and show resorption of the ferromagnesian phases such as olivine, pyroxene and amphibole. Fine-grained resorption zones in plagioclase are probably caused by superheating, as described by Tsuchiyama (1985). The clear overgrowth rims on the sieved cores demonstrate that the reaction took place before crystallization of the inclusion groundmass began. Phenocrysts which are reacted and resorbed in the study area formed when their host magma interacted with a more basic one. The olivine phenocrysts exhibit normal zoning whereas some of the plagioclases are reversely zoned. These features may be generated by fractionation of plagioclase in a magma chamber at depth, with a sudden influx of more primitive phenocryst-poor magma. The result is continuous normal zoning of olivine phenocrysts and reversed zoning of the previously formed plagioclase phenocrysts as a result of the new liquid composition (e.g. more primitive). Whole-rock major and trace element chemistry is also an excellent method of determining mixing relationships (Reid et al. 1983; Srogi & Lutz 1997). Perfect mixing may be identified by linear trends for

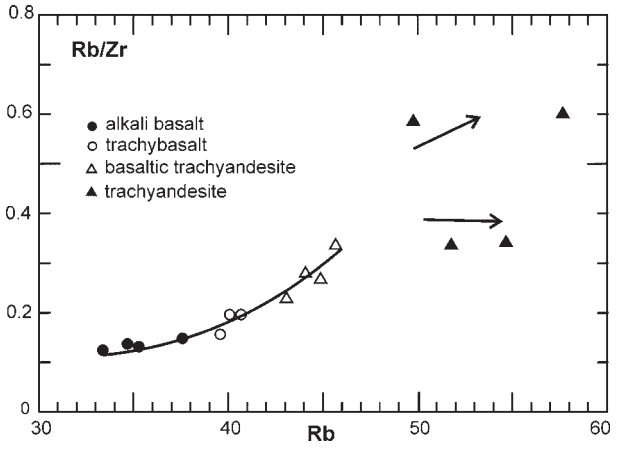

Fig. 14. Rb/Zr variations against Rb for the Ahar Quaternary volcanic rocks.

all elements in Harker diagrams, but nonlinear trends on Harker variation diagrams are consistent with crystal fractionation processes (Wall et al. 1987) (Figs. 5, 6).

It is very difficult to assess the extent of magma mixing if the source was the same for all magmas. However, magma mixing is not believed to be of great importance in the evolution of Ahar magmas, because: (1) the small compositional differences between magma types, (2) the identical isotopic signatures of the erupted lavas, and (3) the domination of normally zoned phenocrysts (olivine and plagioclase) over the occasional reversely zoned plagioclases (4) unlinear trends in Harker diagrams.

Determination of source characteristics

Whole-rock REE content is mainly controlled by source composition and degree of partial melting and as such it has been widely used to determine the origin of the magmas, and the degree of, and variation in mantle melting (e.g. Gurenko & Chaussidon 1995; Johnson 1998; Münker 2000; Green 2006; Zhao & Zhou 2007). The REE are moderately incompatible during melting of mantle peridotite according to their partitioning coefficient (Johnson 1998), and thus, their concentrations and ratios are not greatly affected by mantle depletion and fluid influx (Pearce & Peate 1995; Münker 2000). Sm/Yb ratios can be used to constrain the source mineralogy of the alkaline magmas, since Yb is compatible with garnet. Thus, we have achieved REE modelling of the alkali basalt samples (Fig. 15). In REE modelling, we use the fractional and batch melting equations of Shaw (1970). La, Sm and Yb concentrations, mineral/melt (K_d) and bulk (D_0) partition coeffcients and modal mineralogy of the spinel-peridotite and garnet-peridotite are reported in Tables 3 and 4. The plot of Sm/Yb versus La/Sm and La/Yb distinguishes between melting of garnet- and spinel-peridotite sources (Fig. 15). Partial melting of a spinel-peridotite source produces melts with lower Sm/Yb ratios than a garnet-peridotite source. It is apparent from Figure 15 that the alkali basalt clearly plots on the fractional melting curve of spinel-peridotite. REE modelling indicates that the alkali basalts formed by partial melting of spinel-peridotite sources via degree of partial melting ranging from ~1 % to ~3 %. In Table 5 — trace element contents, bulk distribution coeficients and results obtained from the calculations of 1 % to 5 % fractional melting of the spinel-peridotite are reported. The results obtained from 1 % to 5 % degree of partial melting modelling were compared to the alkali basalt samples on the primitive mantle-normalized spidergram (Fig. 16). It is clear in Figure 16 that the trace element pattern obtained from the 2.5 % fractional melting of the spinel-peridotite sample has the highest similarity to the alkali basalt samples. We conclude that the alkali basalt samples were generated by low degree partial melting (~2.5 %) of a spinel-peridotite source.

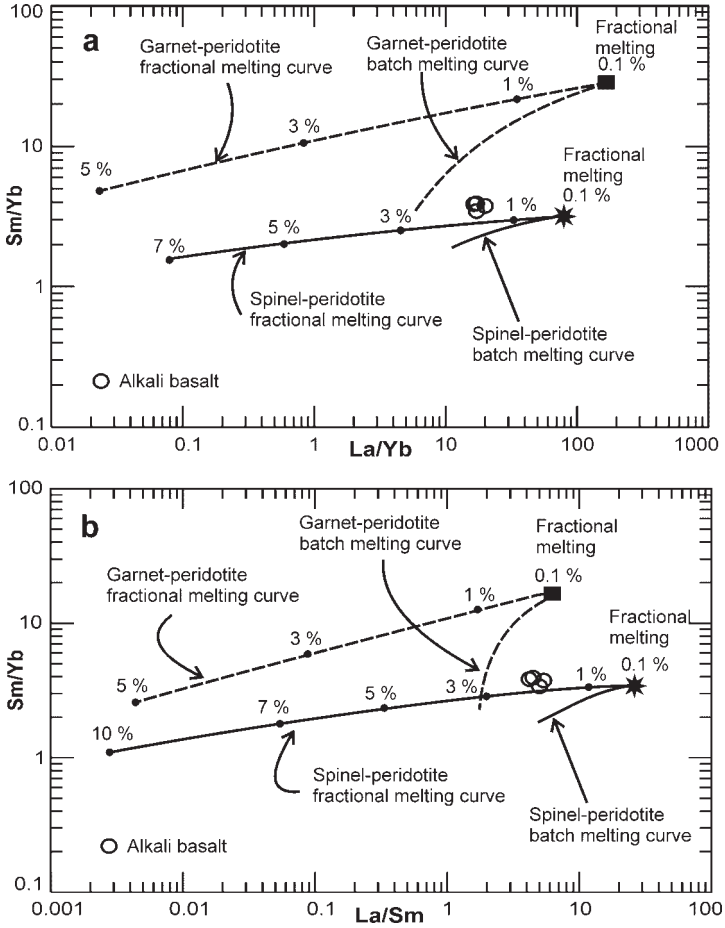

Fig. 15. (**a**) Sm/Yb versus La/Yb and (**b**) Sm/Yb versus La/Sm diagrams showing the melt curves obtained from fractional and batch melting equations of Shaw (1970). La, Sm and Yb concentrations of the spinel and garnet peridotite are from McDonough (1990) and Sen & Leeman (1991), respectively. Bulk partition coefcients are taken from Tables 3 and 4. Solid square and star represent starting compositions of garnet and spinel peridotite at 0.1 % F, respectively.

Table 3: Data used in the batch and fractional melting calculations of spinel-peridotite.

	Spinel-peridotite composition (K_d)	Mineral/melt partition coeficients				Bulk partititon coeficients (D_0) (66 % Ol, 24 % Opx, 8 % Cpx, 2 % Spinel)
	Initial concentration Co (ppm)	Olivine	Opx	Cpx	Spinel	
La	2.6	0.0067	–	0.056	0.01	0.0091
Sm	0.47	0.007	0.05	0.45	0.01	0.053
Yb	0.26	0.014	0.34	0.542	0.01	0.13

La, Sm and Yb concentrations are from McDonough (1990), modal mineralogy of the spinel-peridotite are from Wilson (1989: p. 50) and mineral/melt partition coeficients of the basaltic melts are from Fujimaki, Tatsumoto & Aoki (1984); McKenzie & O'Nions (1991); Rollinson (1993: p. 108). **Abbrevations: Opx** — orthopyroxene; **Cpx** — clinopyroxene; **Ol** — olivine.

Table 4: Data used in the batch and fractional melting calculations of garnet-peridotite.

	Garnet-peridotite composition (K_d)	Mineral/melt partition coeficients				Bulk partititon coeficients (D_0)
	Initial concentration Co (ppm)	Olivine	Opx	Cpx	Garnet	(63 % Ol, 30 % Opx, 2 % Cpx, 5 % Garnet)
La	1.73	0.0067	–	0.056	0.0016	0.0054
Sm	1.12	0.007	0.05	0.45	0.217	0.039
Yb	0.51	0.014	0.34	0.542	6.167	0.43

La, Sm and Yb concentrations are from Sen & Leeman (1991), modal mineralogy of the garnet-peridotite are from Wilson (1989: p. 50) and mineral/melt partition coeficients of the basaltic melts are from Irving & Frey (1978), Fujimaki, Tatsumoto & Aoki (1984); Rollinson (1993: p. 108). **Abbrevations: Opx** — orthopyroxene; **Cpx** — clinopyroxene; **Ol** — olivine.

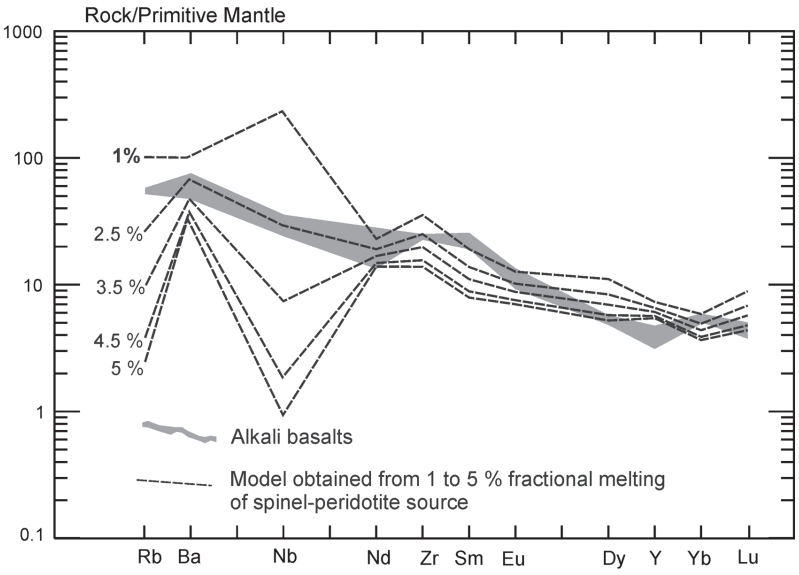

Fig. 16. Primitive mantle normalized (Sun & McDonough 1989) spidergrams calculated from the spinel-peridotite sample (McDonough 1990) at 1 to 5 % fractional melting, compared with the alkali basalt samples. Trace element concentrations and bulk partition coefcient (D_o) of spinel-peridotite are taken from Table 5. Modal mineralogy of the spinel-peridotite as in Table 3.

Table 5: Data obtained from the 1 % to 5 % fractional melting calculations of the spinel-peridotite (McDonough 1990) end-member.

	Starting composition (66 % Ol, 24 % Opx, 8 % Cpx, 2 % Spinel) Spinel-peridotite	Bulk partition coeficients (D_0)	Calculated composition for fractional melting				
			1 %F	2.5 %F	3.5 %F	4.5 %F	5 %F
Rb	1.9	0.01	70.11	17.09	6.59	2.51	1.55
Ba	33	0.04	714.66	469.12	353.05	264.92	229.22
Nb	4.8	0.01	168.48	21.73	5.45	1.35	0.67
Nd	2.67	0.08	31.09	25.82	22.78	20.07	18.83
Zr	21	0.04	397.57	280.65	221.84	174.93	155.19
Sm	0.47	0.053	8.47	6.11	4.91	3.93	3.51
Eu	0.16	0.07	2.13	1.71	1.47	1.27	1.18
Dy	0.51	0.05	8.17	6.18	5.12	4.24	3.85
Y	4.4	0.12	33.27	29.84	27.73	25.75	24.80
Yb	0.26	0.13	2.90	2.43	2.16	1.91	1.80
Lu	0.043	0.06	0.66	0.51	0.42	0.35	0.32

Modal mineralogy of the spinel-peridotite as in Table 3. The mineral/melt partition coefcients of the basaltic melts are from Fujimaki, Tatsumoto & Aoki (1984); McKenzie & O'Nions (1991); Rollinson (1993: p. 108). **Abbrevations: Opx** — orthopyroxene; **Cpx** — clinopyroxene; **Ol** — olivine.

Geodynamic implications

NW Iran is in the central part of the Arabian lithospheric collisional zone, which experienced N–S shortening and E–W extension accompanied by intense faulting, strong earthquakes and active volcanism (e.g. Dewey et al. 1986; Karakhanian et al. 1997; Talebian & Jackson 2002; Karakhanian et al. 2004; Copley & Jackson 2006). This region was affected by a complex tectonic regime from the Late Paleocene–Early Eocene (Şengör & Kidd 1979; Topuz et al. 2005; Karsli et al. 2007; Önal & Kaya 2007). The melt generation modelling and geochemical results presented above show that the source of the alkaline rocks is enriched in LILE and LREE relative to primitive mantle (PM) and depleted MORB mantle (DMM).

Three main geodynamic models have been suggested to explain the melting process of the lithospheric mantle in NW Iran and SE Turkey. They include mantle plume (Ershov & Nikishin 2004), partial lithospheric delamination (Pearce et al. 1990) and slab breakoff (Keskin 2003; Şengör et al. 2003). For NW Iran and the northern part of UDMA, the melting of mantle lithosphere by heat from a mantle plume is improbable, because there is no evidence for a mantle plume origin. Ahar Quaternary volcanic rocks have high $^{87}Sr/^{86}Sr$ and low $^{143}Nd/^{144}Nd$ compared to rocks derived from plumes (e.g. Quaternary Hocheifel lavas (QH)) (Fig. 8). A mantle plume would also be expected to produce a dynamic uplift over an area 1000–2000 km in diameter (White & McKenzie 1989; Hill et al. 1992; Ritter & Christensen 2007). Furthermore, the overall volcanic expression in NW Iran is asymmetrical, extending in a NW–SE trend sub-parallel to the general trend of the orogenic belt. Therefore, a possible cause of the melting of the lithospheric mantle beneath the area can be explained by heat from asthenospheric upwelling resulting from lithospheric delamination or by detachment of subducted slab following collision. Both mechanisms involve ascent of asthenospheric mantle to replace the sinking material. These are not mutually exclusive explanations (Keskin et al. 2006; Dokuz 2010). A partial lithospheric delamination model is suggested by Pearce et al. (1990) for volcanism in Eastern Anatolia and recently by Liotard et al. (2008) for the genesis of Quaternary alkaline volcanic rocks in Damavand volcano. The slab breakoff model is proposed by Keskin (2003) and Şengör et al. (2003) for genesis of collision related Miocene to Quaternary volcanism in

Eastern Anatolia and recently by Ghasemi & Talbot (2006) and Omrani et al. (2008) for Pliocene-Quaternary volcanic rocks at UDMA in the Zagros orogeny.

The northern part of UDMA has experienced calc-alkaline magmatism during the Eocene period and alkaline and ultrapotassic magmatism during the Quaternary period (Ahmadzadeh et al. 2010). Preliminary research indicates that calc-alkaline magmatism during the Eocene is related to subduction of Neo-Tethys oceanic crust beneath CIM. Opening of the Red Sea and the Gulf of Aden and rotation of the Arabian plate has been responsible for oblique convergence between the Arabian plate and CIM and the final closure of the Neo-Tethys Ocean. The final closure of Neo-Tethys and collision between the Arabian plate and CIM took place before or during the Late Miocene (Berberian & Berberian 1981; Berberian et al. 1982; Dargahi 2007). In the northern part of UDMA, cessation of magmatism occurred after the main period of convergence, probably controlled by rollback processes and subsequent breakoff of the subducted slab (Ghasemi & Talbot 2006; Jahangiri 2007). After the calc-alkaline volcanism, an extensional transtensional regime was developed in the Oligocene-Miocene period. As a result of extensional transtensional regime, local volcanic activities occurred along the main dextral faults, like the north-Tabriz dextral fault. The volcanic activity along the north Tabriz dextral fault is represented by the Late Miocene and ultrapotassic and alkaline mafic magmas with adakitic signatures during the Pliocene–Quaternary (Ahmadzadeh et al. 2010).

These variations in the lava chemistry of the Cenozoic volcanic rocks (Eocene to Quaternary) indicate a geochemical progression from calc-alkaline to more alkaline compositions over time and a spatial shift from north to south towards the Arabian plate. Considering the temporal and spatial relationship between calc-alkaline, adakitic, ultrapotassic and alkaline rocks, the northwestern UDMA is a special case of subduction-related, rollback magmatism and was possibly related to a slab breakoff (detachment) system. Slab breakoff leads to the generation of a shallow thermal perturbation and opening of an asthenospheric window that in turn caused partial melting of the subduction metasomatized lithospheric mantle beneath the collision zone (Davies & von Blanckenburg 1995). The findings of the recent northern part of UDMA (Taghizadeh-Farahmand 2010) and eastern Turkey seismic experiment (Al-Lazki et al. 2003; Gök et al. 2003; Zor et al. 2003) and seismic velocity from the Zagros collision to UDMA and CIM (Kaviani et al. 2007), along with the tomographic models, suggest that velocity difference at shallow depth is due to higher mantle temperatures and/or higher fluid content beneath NW Iran and eastern Turkey. These observations, combined with trace element and isotope characteristics of these volcanic sequences, suggest that their magmas were derived from partial melting of subduction-metasomatized continental lithospheric mantle in the spinel-peridotite field beneath the CIM.

Conclusions

The Ahar volcanic rocks range from alkali basalts to trachyandesites and show a typical alkaline differentiation trend. Major and trace element variations indicate fractional crystallization. Alkali basalts crystallized from relatively primitive magma as suggested by their mineralogy, geochemistry and trace element ratios. AFC modelling, as well as trace element ratios indicate that crustal contamination played an important role in petrogenesis of the trachyandesites. The small compositional differences between magma types, identical isotopic signatures, the domination of normally zoned phenocrysts and nonlinear trends on Harker diagrams also suggest that magma mixing is not of great importance in the evolution of the Ahar magmas. Alkali basalts were derived from a spinel-peridotite mantle source via a small degree (~2.5 %) of partial melting.

Acknowledgments: We are grateful to Drs. Patrik Konečný, Jaroslav Lexa and Ioan Seghedi for their constructive reviews that significantly improved the quality of this paper. This article is derived from a PhD Thesis entitled, "Geochemistry and petrology of Quaternary mafic volcanic rocks from NW Ahar, NW Iran". The authors appreciate the support received from the Islamic Azad University, Sciences and Researches Branch.

References

Agard P., Omrani J., Jolivet L. & Mouthereau F. 2005: Convergence history across Zagros (Iran): constraints from collisional and earlier deformation. *Int. J. Earth Sci.* 94, 401–419.

Aghazadeh M. 2009: Petrology and geochemistry of Anzan-Khankandi and Shaivar Dagh granitoids (North and East of Ahar, Eastern Azerbaijan) with references to associated mineralization. *Unpubl. Ph.D. Thesis, Tarbiat Modares University*, 1–446.

Ahmadzadeh G., Jahangiri A., Lentz D. & Mojtahedi M. 2010: Petrogenesis of Plio-Quaternary post-collisional ultrapotassic volcanism in NW of Marand, NW Iran. *J. Asian Earth Sci.* 39, 37–50.

Alavi M. 1994: Tectonics of the Zagros orogenic belt of Iran: new data and interpretations. *Tectonophysics* 229, 211–238.

Alavi M. 2004: Regional stratigraphy of the Zagros fold-thrust belt of Iran and its proforeland evolution. *Amer. J. Sci.* 304, 1–20.

Alberti A.A., Cominhiaramonti P., Sinigoi S., Nicoletti M. & Petrucciani C. 1980: Neogene and Quaternary volcanism in Eastern Azerbaijan (Iran): some K-Ar age determinations and geodynamic implications. *Geol. Rdsch.* 69, 1, 216–225.

Al-Lazki A.I., Seber D., Sandvol E., Turkelli N., Mohamad R. & Barazangi M. 2003: Tomographic Pn velocity and an isotropy structure beneath the Anatolian plateau (eastern Turkey) and the surrounding regions. *Geophys. Res. Lett.* 30, 24, 8043, doi: 10.1029/2003GL017391

Allegre C.J. & Minster J.F. 1978: Quantitative models of trace element behaviour in magnetic processes. *Earth Planet. Sci. Lett.* 38, 1–25.

Amidi S.M., Emami M.H. & Michel R. 1984: Alkaline character of Eocene volcanism in the middle part of Central Iran and its geodynamic situation. *Geol. Rundsch.* 73, 917–932.

Ashrafi N. 2009: Mineralogy, petrology and geochemistry of foid-syenites of East Azarbaijan, NW Iran. *Unpubl. Ph.D. Thesis, Tabriz University*, Iran, 1–190.

Aydin F., Karsli O. & Chen B. 2008: Petrogenesis of the Neogene alkaline volcanics with implications for post-collisional lithospheric thinning of the Eastern Pontides, NE Turkey. *Lithos* 104, 249–266.

Azizi H. & Jahangiri A. 2008: Cretaceous subduction-related volcanism in the northern Sanandaj-Sirjan Zone, Iran. *J. Geodynamics* 45, 178–190.

Azizi H. & Moinevaziri H. 2009: Review of the tectonic setting of Cretaceous to Quaternary volcanism in northwestern Iran. *J. Geodynamics* 47, 167–179.

Babakhani A.R., Lesquyer J.L. & Rico R. 1990: Geological Map of Ahar Quadrangle (scale 1:250,000). *Geol. Surv. Iran*, Tehran, Iran.

Berberian F. & Berberian M. 1981: Tectono-plutonic episodes in Iran. In: Gupta H.K. & Delaney F.M. (Eds.): Zagros, Hindu Kush, Himalaya geodynamic evolution. *Amer. Geophys. Union, Geodynamics Ser.* 3, 5–32.

Berberian F., Muir I.D., Pankhurst R.J. & Berberian M. 1982: Late Cretaceous and early Miocene Andean-type plutonic activity in northern Makran and Central Iran. *J. Geol. Soc. London* 139, 605–614.

Buket E. & Temel A. 1998: Major-element trace-element and Sr–Nd isotopic geochemistry and genesis of Varto (Mus) volcanic rocks, Eastern Turkey. *J. Volcanol. Geotherm. Res.* 85, 405–422.

Copley A. & Jackson J. 2006: Active tectonics of the Turkish-Iranian plateau. *Tectonics* 25, TC6006.

Dargahi S. 2007: Post-collisional Miocene magmatism in the Sarcheshmeh-Shahrebabak region NW of Kerman: Isotopic study, petrogenetic analysis and geodynamic pattern of granitoid intrusives and the role of adakitic magmatism in development of copper mineralization. *Unpubl. Ph.D. Thesis, Shahid Bahonar University of Kerman*, 1–310.

Davidson J.P., Ferguson K.M., Colucci M.T. & Dungan M.A. 1987: The origin of magmas from the San Pedro-Pellado Volcanic Dokhan Volcanics Complex, S Chile: multicomponent sources and open system evolution. *Contr. Mineral. Petrology* 100, 429–445.

Davies J.H. & Von Blanckenburg F. 1995: Slab breakoff, a model of lithosphere detachment and its test in the magmatism and deformation of collisional orogens. *Earth Planet. Sci. Lett.* 129, 85–102.

DePaolo D.J. 1981: Trace element and isotopic effects of combined wallrock assimilation and fractional crystallization. *Earth Planet. Sci. Lett.* 53, 189–202.

Dewey J.F., Hempton M.R., Kidd W.S.F., Saroglu F. & Sengor A.M.C. 1986: Shortening of continental lithosphere: the neotectonics of eastern Anatolia, a young collision zone. In: Coward M.P. & Ries A.C. (Eds.): Collision tectonics. *Geol. Soc.* 19, 3–36.

Dilek Y., Imamverdiyev N. & Altunkaynak S. 2010: Geochemistry and tectonics of Cenozoic volcanism in the Lesser Caucasus (Azerbaijan) and the peri-Arabian region: Collision-induced mantle dynamics and its magmatic fingerprint. *Int. Geol. Rev.* 52, 536–578.

Dokuz A. 2010: A slab detachment and delamination model for the generation of Carboniferous high-potassium I-type magmatism in the Eastern Pontides, NE Turkey: The Köse composite pluton. *Gondwana Res.* (in print, corrected proof, available online 1 October 2010.)

Dupuy C. & Dostal J. 1978: Geochemistry of calc-alkaline volcanic rocks from southeastern Iran (Kouh-e-shahsavaran). *J. Volcanol. Geotherm. Res.* 4, 363–373.

Emami H. 1981: Geologie de la reigon de Qom-Aran (Iran) contribution a l'etude denamique et geochemique du volcanisme Teriaire de l'Iran centaral. *Unpubl. Ph.D. These, University Sc. Et Medical de Grenoble*, 1–489.

Ershov A.V. & Nikishin A.M. 2004: Recent geodynamics of the Caucasus Arabia, East Africa Region. *Geotectonics* 38, 2, 123–136.

Farhoudi G. 1978: A comparison of Zagros geology to island arcs. *J. Geol.* 86, 323–334.

Fekiacova Z., Mertz D.F. & Hofmann A.W. 2007: Geodynamic setting of the Tertiary Hocheifel volcanism (Germany). Part II. Geochemistry and Sr, Nd, Pb isotope compositions. In: Ritter J.R.R. & Christensen U.R. (Eds.): Mantle plumes — A multidisciplinary approach. *Springer*, 205–239.

Fujimaki H., Tatsumoto M. & Aoki K. 1984: Partition coefcients of Hf, Zr and REE between phenocrysts and groundmasses. Proceedings of the fourteenth lunar and planetary science conference. Part 2. *J. Geophys. Res. Suppl.*, B662–72.

Ghasemi A. & Talbot C.J. 2006: A new tectonic scenario for the Sanandaj-Sirjan zone (Iran). *J. Asian Earth Sci.* 26, 683–693.

Gök R., Sandvol E., Turkelli N., Seber D. & Barazangi M. 2003: Sn attenuation in the Anatolian and Iranian plateau and surrounding regions: *Geophys. Res. Lett.* 30, 24, 8043, doi: 10.1029/2003GL018020

Green N.L. 2006: Influence of slab thermal structure on basalt source regions and melting conditions: REE and HFSE constraints form the Garibaldi volcanic belt, northern Cascadia subduction system. *Lithos* 87, 23–49.

Gurenko A.A. & Chaussidon M. 1995: Enriched and depleted primitive melts included in olivine from Icelandic tholeiites: origin by continuous melting of a single mantle column. *Geochim. Cosmochim. Acta* 59, 2905–2917.

Gülen L. 1984: Sr, Nd, Pb, isotope and trace element geochemistry of calc-alkaline and alkaline volcanics, eastern Turkey. *Ph.D. Thesis, Massachusetts Institute of Technology*, USA, 1–232 (unpubl.).

Hajalilou B., Moayyed M. & Hosseinzadeh Gh. 2009: Petrography, geochemistry and geodynamic environment of potassic alkaline rocks in Eslamy peninsula, northwest of Iran. *J. Earth System Sci.* 118, 643–657.

Hart S., Hauri E.H., Oschmann L.A. & Whitehead J.A. 1992: Mantle plumes and entrainment. *Science* 256, 517–520.

Hassanzadeh J. 1993: Metallogenic and tectonomagmatic events in the SE sector of the Cenozoic Active Continental Margin of Central Iran. *University of California*, Los Angeles, 1–204.

Hill R.I., Campbell I.H., Davies G.F. & Griffiths R.W. 1992: Mantle plumes and continental break-up. *Earth Planet. Sci. Lett.* 104, 398–416.

Innocenti F., Mazzuoli R., Pasquare G., Radicati F. & Villari L. 1982: Tertiary and Quaternary volcanism of the Erzurumkars area (Eastern Turkey): Geochronological data and geodynamic evolution. *J. Volcanol. Geotherm. Res.* 13, 3–4, 223–240.

Irvine T.N. & Barager W.R.A. 1971: A guide to the geochemical classification of the common volcanic rocks. *Canad. J. Earth Sci.* 8, 523–548.

Irving A.J. & Frey F.A. 1978: Distributions of trace elements between garnet megacrysts and host volcanic liquids of kimberlitic to rhyolitic composition. *Geochim. Cosmochim. Acta* 42, 771–87.

Jahangiri H. 2007: Post-collisional Miocene adakitic volcanism in NW Iran: Geochemical and geodynamic implications. *J. Asian Earth Sci.* 30, 433–447.

Jamali H., Dilek Y., Daliran F., Yaghubpur A. & Mehrabi B. 2010: Metallogeny and tectonic evolution of the Cenozoic Ahar-Arasbaran volcanic belt, northern Iran. *Int. Geol. Rev.* 2, 608–630.

Johnson K.T.M. 1998: Experimental determination of partition coefficients for rare earth and high-field-strength elements between clinopyroxene, garnet, and basaltic melt at high pressures. *Contr. Mineral. Petrology* 133, 60–68.

Johnson K.T.M., Dick H.J.B. & Shimizu N. 1990: Melting in the oceanic upper mantle: an ion microprobe study of diopsides in abyssal peridotites. *J. Geophys. Res.* 95, 2661–2678.

Jung D., Kursten M. & Tarkian M. 1976: Post-Mesozoic volcanism in Iran and its relation to the subduction of the Afro-Arabian under the Eurasian plate. In: Pilger A. & Rosler A. (Eds.): A far between continental and oceanic rifting. *Schweizerbartsche Verlagbuchhandlung*, Stuttgart, 175–181.

Karakhanian A.S., Djrbashian R.T., Trifonov V.G., Philip H. & Ritz J.F. 1997: Active faults and strong earthquakes of the Armenian

upland — Historical and prehistorical earthquakes in the Caucasus. *Kluwer Academic Publishers*, 181–187.

Karakhanian A.S., Trifonov V.G., Philip H., Avagyan A., Hessami K., Jamali F., Salih Bayraktutan M., Bagdassarian H., Arakelian S., Davtian V. & Adilkhanyan A. 2004: Active faulting and natural hazards in Armenia, Eastern Turkey and northwestern Iran. *Tectonophysics* 380, 189–219.

Karsli O., Chen B., Aydin F. & Şen C. 2007: Geochemical and Sr–Nd–Pb isotopic compositions of the Eocene Dölek and Sariçiçek Plutons, Eastern Turkey: implications for magma interaction in the genesis of high-K calcalkaline granitoids in a post-collision extensional setting. *Lithos* 98, 67–96.

Kaviani A., Paul A., Bourova E., Hatzfeld D., Pedersen H. & Mokhtari M. 2007: A strong seismic velocity contrast in the shallow mantle across the Zagros collision zone (Iran). *Geophys. J. Int.* 171, 399–410.

Keskin M. 1994: Genesis of collision-related volcanism on the Erzurnm-Kars Plateau, Northeastern Turkey. *Ph.D. Thesis, University of Durham*, UK.

Keskin M. 2003: Magma generation by slab steepening and breakoff beneath a subduction-accretion complex: an alternative model for collision-related volcanism in eastern Anatolia. *Geophys. Res. Lett.* 30, 24, 8045, doi:10.1029/2003GL018019

Keskin M., Pearce J.A., Kempton P.D. & Greenwood P. 2006: Magma-crust interactions and magma plumbing in a postcollisional setting: geochemical evidence from the Erzurum-Kars volcanic plateau, eastern Turkey. In: Dilek Y. & Pavlides S. (Eds.): Post-collisional tectonics and magmatism in the Mediterranean region and Asia. *Spec. Pap.* 409, 475–505.

Kheirkhah M., Allen M.B. & Emami M. 2009: Quaternary syn-collision magmatism from the Iran/Turkey borderlands. *J. Volcanol. Geotherm. Res.* 182, 1–12.

Kinzler R.J. 1997: Melting of mantle peridotite at pressure approaching the spinel to garnet transition: application to mid-ocean ridge petrogenesis. *J. Geophys. Res.* 102, 853–874.

Lebedev V.A., Bubnov S.N., Chernyshev I.V., Chugaev A.V., Dudauri O.Z. & Vashakidze G.T. 2007: Geochronology and genesis of subalkaline basaltic lava rivers at the Dzhavakheti highland, Lesser Caucasus: K-Ar and Sr-Nd isotopic data. *Geochem. Int.* 45, 211–225.

Lebedev V.A., Chernyshev I.V. & Dudauri O.Z. 2003: The Samsari volcanic center as an example of recent volcanism in the Lesser Caucasus: K-Ar geochronological and Sr-Nd isotopic data. *Doklady Earth Sci.* 393, 1323–1328.

Le Maitre R.W., Bateman P., Dudek A., Keller J., Lameyre J., Le Bas M.J., Sabine P.A., Schmid R., Sorensen H., Streckeisen A., Woolley A.R. & Zanettin B. 1989: A classification of igneous rocks and glossary of terms: Recommendations of the International Union of Geological Sciences Subcommission on the Systematics of Igneous Rocks. *Blackwell Scientific Publications*, Oxford, U.K.

Liotard J.M., Dautria J.M., Bosch D., Condomines M., Mehdizadeh H. & Ritz J.F. 2008: Origin of the absarokite-banakite association of the Damavand volcano (Iran): trace elements and Sr, Nd, Pb isotope constraints. *Int. J. Earth Sci.* 97, 89–102.

Masson F., Djamour Y., Van Gorp S., Chéry J., Tatar M., Tavakoli F., Nankali H. & Vernant P. 2006: Extension in NW Iran driven by the motion of the South Caspian Basin. *Earth Planet. Sci. Lett.* 252, 180.

McDonough W.F. 1990: Constraints on the composition of the continental lithospheric mantle. *Earth Planet. Sci. Lett.* 101, 1–18.

McKenzie D. & O'Nions R.K. 1991: Partial melt distributions from inversion of rare earth element concentrations. *J. Petrology* 32, 1021–1091.

Mehrpartou M. 1993: Geological map of Varzaghan, scale 1 : 1,000,000. *Geological Survey of Iran*, Tehran.

Mirnejad H., Hassanzadeh J., Cousens B.L. & Taylor B.E. 2010: Geochemical evidence for deep mantle melting and lithospheric delamination as the origin of the inland Damavand volcanic rocks of northern Iran. *J. Volcanol. Geotherm. Res.* 198, 288–296.

Mitchell J. & Westaway R. 1999: Chronology of Neogene and Quaternary uplift and magmatism in the Caucasus: constraints from K-Ar dating of volcanism in Armenia. *Tectonophysics* 304, 3, 157–186.

Mohajjel M. & Fergusson C.L. 2000: Dextral transpression in late-Cretaceous continental collision, Sanandaj–Sirjan Zone, western Iran. *J. Struct. Geol.* 22, 1125–1139.

Mohajjel M., Fergusson C.L. & Sahandi M.R. 2003: Cretaceous–Tertiary convergence and continental collision Sanandaj-Sirjan zone Western Iran. *J. Asian Earth Sci.* 21, 397–412.

Moinevaziri H. 1985: Volcanisme Tértiaire et Quatérnaire en Iran. *Thèse d'Etat*, Paris-Sud Orsay, 1–290.

Mollaei H. 1993: Petrochemistry and genesis of the granodiorite and associated iron-copper skarn deposit of Mazraeh, Ahar, East-Azarbayjan, Iran. *Ph.D. Thesis, University of Roorkee*, 1–278.

Mollaei H., Sharma R. & Pe-Piper G. 2009: Copper mineralization around the Ahar Batholith, north of Ahar (NW Iran): evidence for fluid evolution and the origin of the skarn ore deposit. *Ore Geol. Rev.* 35, 401–414.

Moradian A., Peacock S.M. & Rushmer T. 1997: Geochemistry, eochronology and petrography of feldspathoid bearing rocks in Urumieh-Dokhtar Volcanic Belt, Iran. *Unpubl. Ph.D. Thesis, University of Wollongong*, Australia, 1–412.

Münker C. 2000: The isotope and trace element budget of the Cambrian Devil River Arc System, New Zealand: identification of four source components. *J. Petrology* 41, 759–788.

Nakamura N. 1974: Determination of REE, Ba, Fe, Mg, Na, and K in carbonaceous and ordinary chondrites. *Geochim. Cosmochim. Acta* 38, 757–775.

Omrani J., Agard P., Whitechurch H., Benoit M., Prouteau G. & Jolivet L. 2008: Arc-magmatism and subduction history beneath the Zagros mountains. A new report of adakites and geodynamic consequences. *Lithos* 106, 380–398.

Önal M. & Kaya M. 2007: Stratigraphy and tectono-sedimentary evolution of the Upper Cretaceous–Tertiary sequence in the southern part of the Malatya Basin, East Anatolia, Turkey. *J. Asian Earth Sci.* 29, 878–890.

Pearce J.A. 1983: Role of the sub-continental lithosphere in magma genesis at active continental margins. In: Hawkesworth C.J. & Norry M.J. (Eds.): Continental basalts and mantle xenoliths. *Shiva*, Nantwich, 230–249.

Pearce J.W. & Peate D.W. 1995: Tectonic implications of the composition of volcanic arc magmas. *Ann. Rev. Earth Planet. Sci.* 23, 251–285.

Pearce J.A., Bender J.F., De Long S.E., Kidd W.S.F., Low P.J., Güner Y., Saroglu F., Yilmaz Y., Moorbath S. & Mitchell J.G. 1990: Genesis of collision volcanism in Eastern Anatolia, Turkey. *J. Volcanol. Geotherm. Res.* 44, 189–229.

Reid J.B., Evans O.C. & Fates D.G. 1983: Magma mixing in granitic rocks of the central Sierra Nevada, California. *Earth Planet. Sci. Lett.* 66, 243–26.

Richards J.P. 2003: Metallogeny of the Neo-Tethys arc in central Iran. In: Eliopoulos et al. (Eds.): Mineral exploration and sustainable development. *7th Biennial SGA Meeting, Athens, August 24–28. Millpress*, Rotterdam, 1237–1239.

Ricou L.E. 1994: Tethys reconstructed: plates, continental fragments and their boundaries since 260 Ma from Central America to South-eastern Asia. *Geodinamica Acta* 7, 169–218.

Ritter J.R.R. & Christensen U.R. (Eds.) 2007: Mantle Plumes — A multidisciplinary approach. *Springer Verlag*, Heidelberg, 1–502.

Rollinson H.R. 1993: Using geochemical data: Evaluation, presentation, interpretation. *Longman*, UK, 1–352.

Rutherford M.J. & Hill P.M. 1993: Magma ascent rates from amphibole breakdown: an experimental study applied to the 1980–1986 Mount St Helens eruptions. *J. Geophys. Res.* 98, 19667–19685.

Saadat S. & Stern Ch. 2011: Petrochemistry and genesis of olivine basalts from small monogenetic parasitic cones of Bazman stratovolcano, Makran arc, southeastern Iran. *Lithos*, (in print).

Saadat S., Karimpour M.H. & Stern Ch. 2010: Petrochemical characteristics of Neogene and Quaternary alkali olivine basalts from the Western Margin of the Lut Block, Eastern Iran. *Iranian J. Earth Sci.* 2, 87–106.

Saki A. 2010: Proto-Tethyan remnants in northwest Iran: Geochemistry of the gneisses and metapelitic rocks. *Gondwana Res.* 17, 704–714.

Sen G. & Leeman W.P. 1991: Iron-rich lherzolitic xenoliths from Oahu: origin and implications for Hawaiian magma sources. *Earth Planet. Sci. Lett.* 102, 45–57.

Sosson M., Rolland Y., Corcini M., Danelian T., Stephan J.F., Avagyan A., Melkonian R., Jrbashian R., Melikian L. & Galoian G. 2005: Tectonic evolution of Lesser Caucausus (Armenia) revisited in the light of new structural and stratigraphic results. *Geophys. Res.* 7, p. 06224.

Srogi L. & Lutz T.M. 1997: Chemical variation in plutonic rocks caused by residual melt migration: Implications for granite petrogenesis. In: Sinha A.K., Whalen J.B. & Hogan J.P. (Eds.): The nature of magmatism in the Appalachian Orogen. *Geol. Soc. Amer*., Boulder, Colorado 191, 309–335.

Stocklin J. 1974: Possible ancient continental margins in Iran. In: Burk C.A. & Drake C.L. (Eds.): The geology of continental margins. *Springer*, Berlin, 873–887.

Sun S.S. & McDonough W.F. 1989: Chemical and isotopic systematics of oceanic basalts: implications for mantle composition and processes. In: Saunders A.D. & Norry M.J. (Eds.): Magmatism in Ocean Basins. *Geol. Soc. London*, *Spec. Publ.* 42, 313–345.

Şengör A.M.C. & Kidd W.S.F. 1979: Post-collisional tectonics of the Turkish-Iranian plateau and a comparison with Tibet. *Tectonophysics* 55, 361–376.

Şengör A.M.C. & Yilmaz Y. 1981: Tethyan evolution of Turkey: a plate tectonic approach. *Tectonophysics* 75, 181–241.

Şengör A.M.C., Özeren S., Zor E. & Genç T. 2003: East Anatolian high plateau as a mantle-supported, N–S shortened domal structure. *Geophys. Res. Lett.* 30, 24, 8045, doi:10.1029/2003GL017858

Taghizadeh-Farahmand F., Sodoudi F., Afsari N. & Ghassemi M.R. 2010: Lithospheric structure of NW Iran from P and S receiver functions. *J. Seismology* 14, 4, 823–836.

Tajbakhsh G.R. 2010: Petrology and geochemistry of nepheline syenite of Kaleybar and gabbro-pyroxenite massif of Hashtsar — East Azarbaijan. *Unpubl. Ph.D. Thesis, Tarbiat Modares University*, 1–333.

Talebian M. & Jackson J.A. 2002: Offset on the main recent fault of NW Iran and implications for the late Cenozoic tectonics of the Arabia-Eurasia collision zone. *Geophys. J. Int*. 150, 2, 422–439.

Topuz G., Altherr R., Schwarz W.H., Siebel W., Satir M. & Dokuz A. 2005: Post-collisional plutonism with adakite-like signatures: the Eocene Saraycik granodiorite (Eastern Pontides, Turkey). *Contr. Mineral. Petrology* 150, 441–455.

Tsuchiyama A. 1985: Dissolution kinetics of plagioclase in the melt of the system diopside-albite-anorthite and origin of dusty plagioclase in andesites. *Contr. Mineral. Petrology* 89, 1–16.

Wall V.J., Clemens J.D. & Clark D.B. 1987: Models for granitoid evolution and source compositions. *J. Geol.* 95, 731–749.

Walter M.J. 1998: Melting of garnet peridotite and the origin of komatiite and depleted lithosphere. *J. Petrology* 39, 29–60.

White W.M. & McKenzie D.P. 1989: Magmatism at rift zone: the generation of volcanic continental margins and flood basalts. *J. Geophys. Res.* 94, 7685–7729.

Wilson M. 1989: Igneous petrogenesis. *Unwin Hyman Ltd*., London, 1–465.

Zhao J.H. & Zhou M.F. 2007: Geochemistry of Neoproterozoic mafic intrusions in the Panzhihua district (Sichuan Province, SW China): implications for subduction related metasomatism in the upper mantle. *Precambrian Res.* 152, 27–47.

Zindler A. & Hart S.R. 1986: Chemical geodynamics. *Ann. Rev. Earth Planet. Sci.* 14, 493–571.

Zor E., Sandvol E., Gurbuz C., Turkelli N., Seber D. & Barazangi M. 2003: The crustal structure of the East Anatolian plateau (Turkey) from receiver functions. *Geophys. Res. Lett.* 30, 24, 8043, doi: 10.1029/2003GL018192